Relation of Atlantic tropical cyclone activity with observed and predicted ENSO indices

Michael K. Tippett[1], **Emily J. Becker**[2], **Suzana J. Camargo**[3], **Jorge L. García-Franco**[4], **Chia-Ying Lee**[5], **Michelle L. L'Heureux**[6]

[1]Department of Applied Physics and Applied Mathematics, Columbia University, New York, NY, USA
[2]University of Miami Rosenstiel School for Marine, Earth, and Atmospheric Science, Miami, FL, USA
[3]Columbia Climate School, Columbia University, New York, NY, USA
[4]Escuela Nacional de Ciencias de la Tierra, UNAM, Mexico
[5]Lamont-Doherty Earth Observatory, Columbia University, Palisades, NY, USA
[6]NOAA/NWS/NCEP/Climate Prediction Center, College Park, MD, USA

Key Points:

- Modern ENSO indices outperform the traditional Niño-3.4 index in terms of their association with Atlantic tropical cyclone activity
- The modern ENSO indices show stronger links to central Pacific convection and tropical cyclone-related conditions in the Atlantic
- Forecasts of Atlantic tropical cyclone activity based on the modern ENSO indices have higher skill than ones based on Niño-3.4

Corresponding author: M. K. Tippett, mkt14@columbia.edu

Abstract

El Niño-Southern Oscillation (ENSO) influences global climate variability, including Atlantic tropical cyclone activity. The Niño-3.4 index has long been used to characterize ENSO. However, new ENSO indices have been proposed in recent years. Here, in the context of Atlantic tropical cyclone activity, we compared Niño-3.4 to three modern ENSO indices: the relative Niño-3.4 index, the ENSO Longitudinal Index (ELI), and a Pacific sea surface temperature zonal gradient index. We examined the association of their August–October values with central Pacific convection, tropical cyclone-related variables in the Atlantic (e.g., vertical wind shear and potential intensity), and Atlantic tropical cyclone activity. We also assessed the skill of seasonal forecasts of the ENSO indices and the skill of index-based forecasts of Atlantic tropical cyclone activity. We found that the modern ENSO indices outperform the traditional Niño-3.4 index in nearly all aspects, with the relative Niño-3.4 index showing statistically significant advantages in many cases.

Plain Language Summary

El Niño-Southern Oscillation (ENSO) is a recurring climate pattern in the tropical Pacific Ocean that influences weather and climate around the world, including hurricane activity in the Atlantic. For decades ENSO has been tracked using the "Niño-3.4" index, based on sea surface temperatures in the equatorial Pacific. However, new "modern" ENSO indices have been developed to better capture changes in where and how ENSO events develop, and to account for long-term warming in the tropics. We compared the traditional Niño-3.4 index to three modern indices: the relative Niño-3.4 index, the ENSO Longitudinal Index, and a Pacific Ocean temperature-gradient index—using August–October seasonal means. We examined how each relates to atmospheric conditions over the Pacific, to environmental factors that affect hurricanes in the Atlantic (such as wind shear and potential intensity), and to the number and strength of hurricanes. We also tested how well each index can be predicted in advance by seasonal climate forecast models, and how this translates into skill for seasonal hurricane outlooks. The modern indices provided an overall stronger link to hurricane-related conditions in the Atlantic and to observed hurricane activity. In many cases, they also offered better seasonal forecast performance than the traditional Niño-3.4 index.

1 Introduction

Remote and local climate conditions influence seasonal Atlantic tropical cyclone activity. In particular, ENSO variability in the tropical Pacific plays a role in determining seasonal Atlantic tropical cyclone activity (Lin et al., 2020) by modulating vertical wind shear over the Atlantic (Goldenberg & Shapiro, 1996) and through tropospheric temperature teleconnections (Tang & Neelin, 2004). Consequently, ENSO is a key factor in seasonal predictions of Atlantic tropical cyclone activity (Gray et al., 1993; Klotzbach, 2007; Klotzbach et al., 2017; Vecchi et al., 2010; Villarini et al., 2010) and in explanations of year-to-year variability (Klotzbach et al., 2024; Saunders et al., 2020). ENSO conditions are typically summarized by sea surface temperature (SST) indices, with the Niño-3.4 index and its seasonal counterpart the Oceanic Niño Index (ONI) being most commonly used (Barnston et al., 1997; Kousky & Higgins, 2007).

Although Niño-3.4 has been the default ENSO index for decades, modern ENSO indices have been introduced in recent years to capture additional aspects of ENSO variability and to account for a changing climate. For instance, ENSO events exhibit event-to-event diversity in their east-west location and structure (Kao & Yu, 2009; Capotondi et al., 2014) which is not explicitly accounted for in the Niño-3.4 index. The ENSO Longitudinal Index (ELI; Williams & Patricola, 2018) is designed to represent this diversity by providing an estimate of the average longitude of tropical deep convection. ELI is computed from SST using the approximation that tropical precipitation occurs where relative SST (SST with the tropical mean SST subtracted) is positive (e.g., Izumo et al., 2020). Long-term warming trends and their impact on 30-year climatologies raise issues for the traditional Niño-3.4 index. The relative Niño-3.4 index (the difference of the Niño-3.4 index with the tropical mean SST) addresses these issues by its use of relative SST, which at the same time provides a theory-based connection to convection in the ENSO region (L'Heureux et al., 2024; Van Oldenborgh et al., 2021).

Indices based on Pacific zonal SST gradients have received considerable attention recently because of discrepancies between their observed and modeled long-term trends and the resulting uncertainty for projections of tropical cyclone risk (S. Lee et al., 2022; Seager et al., 2022; Sobel et al., 2023). On interannual timescales, zonal SST gradients are a key element in the Bjerknes feedback whereby a reduction of the east-west tropical Pacific SST gradient during El Niño conditions weakens the low-level equatorial easterlies, leading to reduced upwelling and further SST warming in the east. Despite the important role of the east-west tropical SST gradient, only a few studies have adopted zonal SST gradient indices to represent ENSO (Hoell & Funk, 2013).

Several studies have examined the relationship of ELI with tropical cyclone activity. Williams and Patricola (2018, their Table S5;) found higher correlations of ELI with seasonal Atlantic tropical cyclone activity over the period 1950–2015 than when using Niño-3.4. In particular, they found correlations of -0.33 (Niño-3.4) vs. -0.35 (ELI) for accumulated cyclone energy (ACE) and -0.37 (Niño-3.4) vs. -0.41 (ELI) for number of hurricanes. In terms of global tropical cyclone activity 1990–2021, Klotzbach, Wood, Schreck III, et al. (2022) found significant correlations between seasonal values of ELI and eastern North Pacific ACE ($r = 0.47$), western North Pacific ACE ($r = 0.76$), North Atlantic ACE ($r = -0.51$), and South Pacific ACE ($r = 0.66$). ELI has also appeared in diagnostic studies—for instance, those of the 2020 and 2023 Atlantic hurricane seasons (Klotzbach, Wood, Bell, et al., 2022; Klotzbach et al., 2024).

Despite their promise, several questions regarding the modern ENSO indices remain to be fully addressed. For instance, how does the association of modern ENSO indices with core ENSO phenomena such as central Pacific convection compare with that of the traditional Niño-3.4 index? Although relative Niño-3.4 approximates convection in the Niño-3.4 area, might some other weighting (e.g., by precipitation) of the tropical mean SST improve the approximation (Sobel et al., 2002; Fueglistaler et al., 2015; Izumo et al., 2020)? In the context of Atlantic tropical activity, how do the modern ENSO indices compare to Niño-3.4 in terms of their correlation with Atlantic tropical cyclone-relevant environmental variables and with measures of seasonal Atlantic tropical cyclone activity? How far in advance can the modern ENSO indices be skillfully predicted by current seasonal forecast systems? To date, this question has only been examined for relative Niño-3.4 (L'Heureux et al., 2024). What are the trade-offs between the strength of observed (simultaneous) relations of ENSO indices with Atlantic tropical cyclone activity and the level of skill with which the ENSO indices can be predicted in advance? Finally, given the high level of correlation between the ENSO indices, are detected differences between the indices statistically significant in any sense?

Here we addressed several of the questions and gaps identified above. We first examined the correlation of the ENSO indices with central Pacific outgoing long-wave radiation (CP-OLR), focusing on a previously identified ENSO-related region (L'Heureux et al., 2015) that is highly correlated with precipitation in the deep tropics (Li et al., 2023, their Figure 3) and exploring alternative weighting of the tropical mean SST. To compare how well the ENSO indices capture the downstream responses in the ENSO-Atlantic tropical cyclone teleconnection, we computed their correlation with a tropical cyclone genesis potential index (and its constituent variables) and with seasonal measures of Atlantic tropical cyclone activity. We assessed the skill of North Amer-

ican Multimodel Ensemble (NMME) forecasts of August-October values of the ENSO indices and the skill of the corresponding ENSO-based tropical cyclone activity forecasts, thereby providing a measure of index utility that includes predictability. We used a rigorous statistical method in our comparisons.

2 Data and methods

We computed August–October (ASO) values of the ENSO indices in four SST datasets: ERSSTv5 (Huang et al., 2017), ERA5 (Hersbach et al., 2020), HADISST (Rayner et al., 2003), and COBE2 (Hirahara et al., 2014). Most of the results in the main text use ERSSTv5 and the period 1979–2024. ENSO indices were computed as follows:

- Niño-3.4 is the area-weighted average of SST in the box 170 °W–120 °W, 5 °S–5 °N;
- relative Niño-3.4 is the Niño-3.4 index minus the 20 °S–20 °N tropical mean SST; no rescaling is applied;
- the Pacific zonal gradient is the difference between the eastern Pacific (180 °–80 °W, 5 °S–5 °N) and the western Pacific (110 °E–180 °, 5 °S–5 °N; Watanabe et al., 2021);
- ELI is the average of Pacific basin longitudes 5 °S–5 °N where the SST is greater than or equal to the 5 °S–5 °N tropical mean SST (Williams & Patricola, 2018).

ASO values of the ENSO indices over the period 1950–2024 are visually similar in all four SST datasets except for the systematically lower values of the Niño-3.4 index prior to the mid 1980s (Fig. S1). The lower Niño-3.4 values reflect the fact that trends in ASO Niño-3.4 are positive (1950–2024) or near zero (1979–2024), while trends in the modern ENSO indices are negative. None of the trends are statistically significant at the 5% level (not shown). However, trends in the difference of the modern ENSO indices with Niño-3.4 are statistically significant in all four SST datasets for both the 1950–2024 and 1979–2024 periods (Fig. S2). Despite their differing trends and formulations, the pairwise correlation between ENSO indices exceeds 0.92 in all four datasets for the period 1979–2024. (Fig. S3). Notably ELI, which is a longitudinal measure, has correlations with Niño-3.4 that range from 0.96 to 0.98 depending on SST dataset. The pairwise correlation across datasets of the ENSO indices exceeds 0.97 for the period 1979–2024 which indicates that the indices over this period are fairly insensitive to the choice of dataset (Figure S4).

We computed forecast ASO values of the ENSO indices from the North American Multimodel Ensemble (NMME; Kirtman et al., 2014; Becker et al., 2022). The NMME comprises seven forecast systems: COLA-RSMAS-CCSM4, COLA-RSMAS-CESM1, CanESM5, GEM5.2-NEMO, GFDL-SPEAR, NASA-GEOSS2S, and NCEP-CFSv2. We took ASO forecasts from the period 1991–2024 during which the forecasts (a mixture of real-time forecasts and reforecasts) are complete. NMME forecasts are nominally initialized on the first of each month (start date). The shortest lead forecasts have a start date of August 1, and the longest lead forecasts have a start date of November 1. The multimodel mean forecast is the mean of the ensemble averages of the individual models.

Emanuel's genesis potential index (GPI; Emanuel & Nolan, 2004; Camargo et al., 2007) is a measure of the favorability of environmental conditions for tropical cyclone formation and was computed from absolute vorticity at 850 hPa, vertical wind shear (magnitude of the vector difference of the zonal wind at 200 hPa and 850 hPa monthly averages), potential intensity (PI), and relative humidity at 600 hPa using ERA5 data at 0.25° grid spacing (Hersbach et al., 2020). PI was computed following the Bister and Emanuel (2002) algorithm.

OLR data were taken from the OLR-Monthly CDR Product (Ver03Rev00) available on a global 2.5 ° latitude $\times$ 2.5 ° longitude grid (H.-T. Lee et al., 2007). The CP-OLR index is the average of values in the box 5 °S–5 °N, 170 °E–140 °W.

Atlantic tropical cyclone data were taken from the International Best Track Archive for Climate Stewardship (IBTrACS; Knapp et al., 2010; Gahtan et al., 2024). Only June–November data were considered, and only storm data rated "tropical storm" and greater on the Saffir-Simpson scale were used. This filtering corresponds to storms with USA_WIND $\geq$ 35 knots and NATURE = TS (tropical) and excludes storms classified as disturbance, extratropical, and subtropical. The measures of tropical cyclone seasonal activity considered are: number of tropical storms, number of hurricanes reaching category one and higher denoted Cat1+, ACE (sum of squared 6-hourly wind speeds at 0, 6, 12, and 18 UTC). Time series are shown in Figure S5.

Since we compared the correlation of ENSO indices with the same quantity of interest (e.g., number of tropical storms), the sample correlations are dependent, and comparison based on Fisher-transformed correlations is inappropriate (DelSole & Tippett, 2014). Comparing two correlations is equivalent to comparing the fit of two linear regressions. Therefore, we used the Wilcoxon signed-rank test to decide the statistical significance of differences in squared regression residuals. The idea of the test is to form differences of the (paired) squared residuals, compute signed ranks (ranked

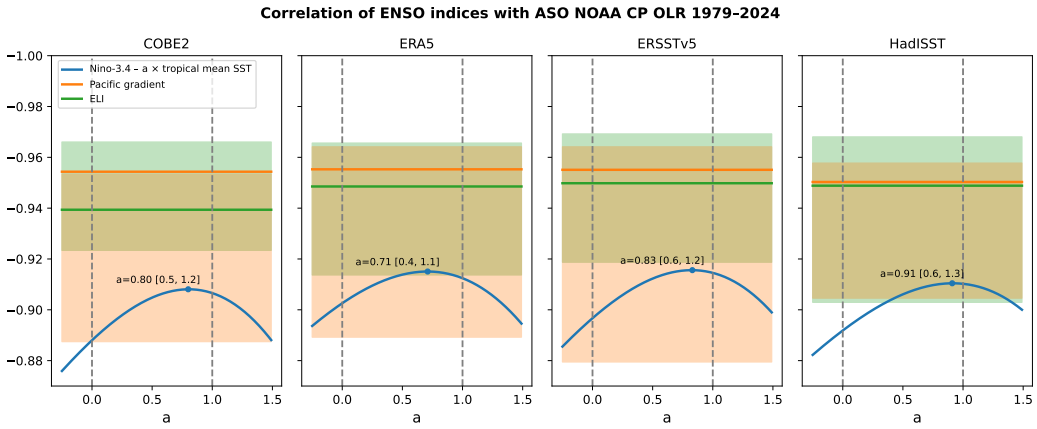

Figure 1. Correlation of ASO CP-OLR with Niño-3.4 – a × tropical mean SST (blue), Pacific gradient (orange), ELI (green) during the period 1979–2024 in four SST datasets. Text shows the value of a that maximizes the correlation (marked by a dot) along with 95% confidence intervals. Orange and green shading shows 95% confidence intervals for the Pacific gradient and ELI correlations, respectively.

by absolute value and then signs attached), and sum the signed ranks. Under the null hypothesis that the residuals come from the same distribution, these sums will be approximately the same. The Wilcoxon signed-rank test is robust to outliers and non-normal distributions, is more powerful than the sign test when the data are symmetric, makes use of the magnitude of differences unlike the sign test which does not, and for symmetric data effectively tests whether the median difference between the squared residuals is zero.

We used bootstrap sampling (1000 samples with replacement) to compute 95% confidence intervals for the correlations of ELI and the Pacific gradient with CP-OLR. To see the roles of local SST (Niño-3.4) and nonlocal SST (tropical mean), we followed Swanson (2008) and correlated CP-OLR with Niño-3.4 minus a varying coefficient a × the tropical mean. The traditional and relative Niño-3.4 indices correspond to $a = 0$ and $a = 1$, respectively. We used bootstrap sampling to compute 95% confidence intervals for the value of a that gives the strongest correlation of CP-OLR with Niño-3.4 - a × (tropical mean SST).

3 Results

To examine the strength of association of the ENSO indices with ENSO-related tropical Pacific convection, we computed the correlation of the ENSO indices with CP-OLR (Figure 1). In all four SST datasets, the Pacific zonal gradient index has the strongest correlation with CP-

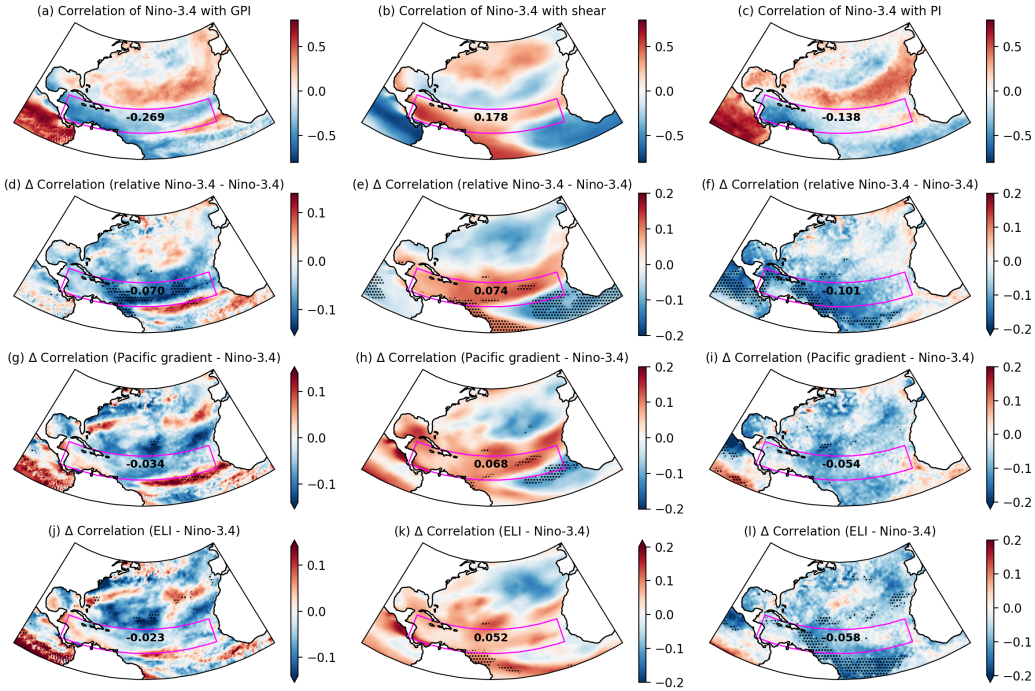

Figure 2. Each column corresponds to one Atlantic environmental variable: GPI (left), vertical wind shear (middle), and potential intensity (PI) (right). The top row (a–c) shows the correlation with Niño-3.4 for ASO 1979–2024. Moving down each column, rows 2–4 show the difference in correlation compared to that of Niño-3.4 when using (d–f) relative Niño-3.4, (g–i) Pacific gradient, and (j–l) ELI. The MDR is outlined in magenta; annotated numbers are MDR averages (correlation in row 1, change in correlation in rows 2–4). Stippling marks statistically significant (5%) differences.

OLR, closely followed by that of ELI. The Pacific zonal gradient and ELI correlations are nearly indistinguishable in the HADISST dataset. In all four SST datasets, the a that optimizes the correlation of CP-OLR with Niño-3.4 – $a \times$ tropical mean SST is less than one, and the 95% confidence intervals for the optimal a contain one and do not contain zero, which is evidence that relative Niño-3.4 ($a = 1$) has a stronger relation with CP-OLR than the traditional Niño-3.4 index does. The same qualitative results were seen in the more recent period 1991–2024 (Figure S6). Correlation maps of Pacific OLR with ENSO indices also show broadly stronger correlations with the modern indices (Figure S7). We used relative Niño-3.4 ($a = 1$) in the remainder of our analysis.

Niño-3.4 shows negative correlations with GPI across the MDR that extend into the western portion of the Gulf of Mexico (Fig. 2a). Positive correlations are present to the north of the

MDR and extend westward from the coast of Africa, where climatologically GPI, ACE, and genesis frequency are relatively low. The modern indices have stronger negative correlations on average with GPI in the MDR than does Niño-3.4 (Figure 2), with relative Niño-3.4 having the greatest advantage. Stronger relations with vertical wind shear and PI are the leading contributors to the advantage of the modern indices. The ENSO signal in vertical shear is strongest in 200 hPa zonal wind, where all the modern ENSO indices have larger MDR average correlations than does Niño-3.4 (Fig. S8). Correlations with 850 hPa zonal wind are negative, with a modest edge to the modern indices, which further contributes to their stronger relation with vertical wind shear. The correlation gain of the modern ENSO indices in 850 hPa absolute vorticity is slight. 600 hPa relative humidity is the GPI ingredients with the highest MDR-averaged correlation with Niño-3.4, but only relative Niño-3.4 shows a correlation improvement with it (Figure S9). Relative Niño-3.4 has the largest lead of the modern indices over Niño-3.4 in terms of MDR-averaged correlations of GPI ingredients.

To examine the strength of association of ENSO indices with Atlantic tropical activity, we computed correlations and scatterplots of the indices with number of tropical storms, number of Cat1+ hurricanes, and ACE (Figure 3). The relative Niño-3.4 index has higher correlations and smaller RMSEs than does the traditional Niño-3.4 index. The advantage of relative Niño-3.4 over the traditional index is statistically significant (5% level) for the number of tropical storms and ACE in all four SST datasets and for Cat1+ in two SST datasets at the 5% level and in the remaining two SST datasets at the 10% level (Figs. S10–S12). The years when ASO traditional and relative Niño-3.4 anomalies (with respect to the 1979–2024 mean) differed most are the years with largest (in absolute value) ASO tropical mean SST anomalies. The top four such years are 2023, 2015, 2024, and 1985 (filled circles in Fig. 3). Atlantic tropical activity values for 2024 are closer to the best-fit line for the modern indices, and in 2023 and 1985 they are also closer to the best-fit line for relative Niño-3.4. ELI and relative Niño-3.4 have nearly the same correlations and RMSEs, with p-values slightly favoring relative Niño-3.4, depending on SST dataset. Although the Pacific gradient index has slightly larger correlations and smaller RMSE than relative Niño-3.4, p-values are mostly larger, indicating less evidence for differences with Niño-3.4. This outcome is possible because the signed-rank test uses ranks and rewards consistency.

For June, July, and August starts, individual model and multimodel mean correlation skill lies below that of persistence for forecasts of all the ENSO indices (Figs. 4a–e). For starts prior to June, the persistence correlation of the ENSO indices drops sharply due to the spring predictability/persistence barrier, and the NMME forecasts have a clear advantage. The skill of tropical mean

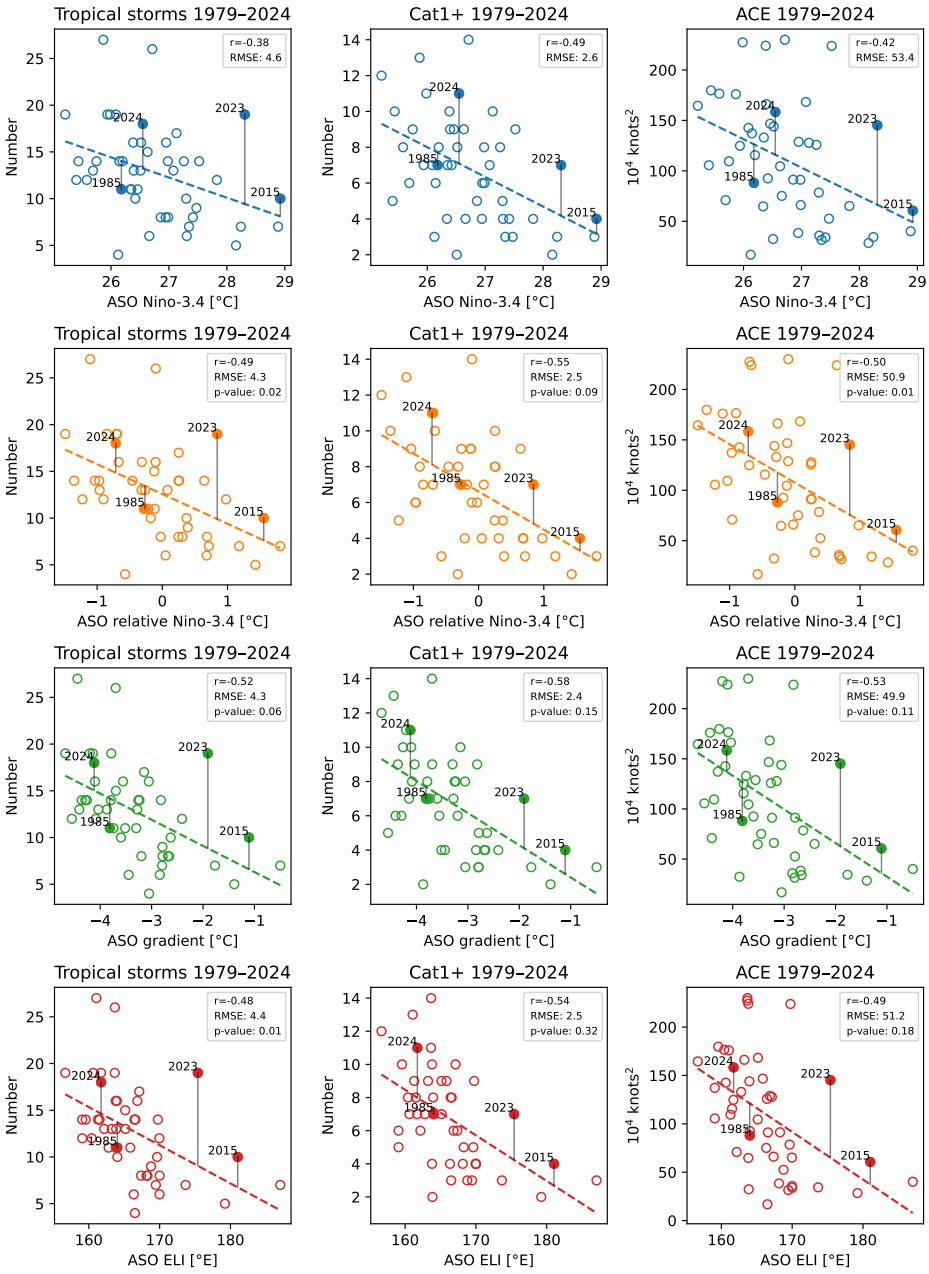

Figure 3. ASO ENSO indices (ERSSTv5) with seasonal number of tropical storms, Cat1+ hurricanes, and ACE for the period 1979–2024, along with best-fit lines (dashed). Vertical lines to the best-fit line are shown for the four years 2023, 2015, 2024, and 1985 with the largest ASO tropical mean SST anomalies (largest to smallest). P-values are shown for the null hypothesis that the relation with Niño-3.4 is the same as with the modern index (small values favor rejecting).

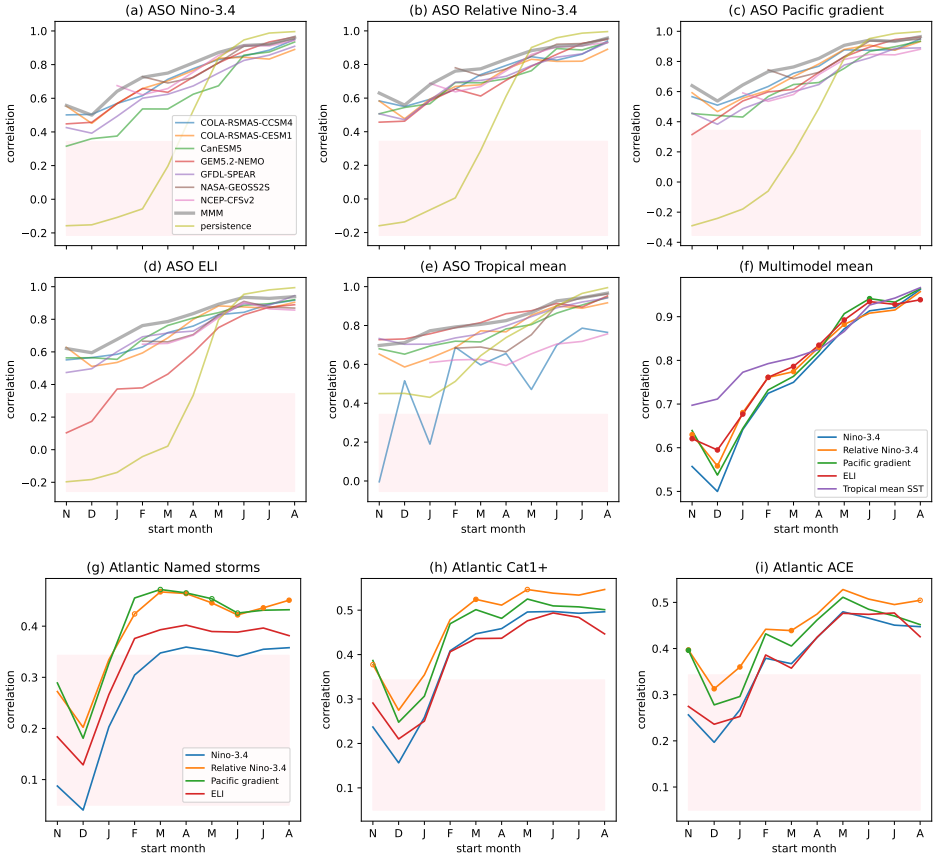

Figure 4. NMME correlation skill (target period 1991–2024; ERSSTv5 verification) for predicting ASO (a) Niño-3.4, (b) relative Niño-3.4, (c) Pacific gradient, (d) ELI, and (e) tropical mean SST as a function of start month (November of previous year though August of target year) along with (f) multimodel ensemble mean (MMM) skill. Correlation skill for MMM ENSO index-based forecasts of seasonal Atlantic (g) number of named storms, (h) number of Cat1+ hurricanes, and (i) ACE as a function of start month. Pink shading shows statistically insignificant skill. Dots in panels (f)–(i) indicate statistically significant differences in the skill of the modern indices compared to that of Niño-3.4 at the 5% level (filled) and 10% level (open).

SST forecasts drops off more slowly than that of ENSO forecasts. Two models (CFSv2 and CCSM4; they share initial conditions) have markedly lower skill in predicting the tropical mean but that issue does not seem to impact their forecasts of relative Niño-3.4. In the multimodel mean, correlation forecast skill of the different ENSO indices is fairly similar though the skill for ELI is significantly lower than that of Niño-3.4 for August starts (Fig. 4f). From May starts on, relative Niño-3.4 and ELI are forecast with significantly higher skill in the multimodel mean than is Niño-3.4.

To evaluate the trade-off between the predictability of ENSO indices and their ability to capture observed relationships with Atlantic tropical cyclone activity, we computed the correlation of forecast indices with Atlantic tropical storm activity (Figs. 4g–i). The forecast ENSO indices have statistically significant correlations with Atlantic ACE and numbers of tropical and hurricanes for starts as early as February. Forecasts of relative Niño-3.4 and Pacific gradient have the highest correlation with tropical cyclone activity at most lead times, and their advantage over Niño-3.4 is sporadically significant for forecasts of the number of Atlantic tropical storms.

4 Summary and discussion

For over three decades, sea surface temperature in the Niño-3.4 region has been recognized as a key measure of ENSO conditions. However, in recent years new ENSO indices have been proposed that offer potential advantages over the traditional Niño-3.4 index. The relative Niño-3.4 index accounts for tropical warming by using relative SST (local SST minus tropical mean SST), which provides a theory-based connection to tropical convection. The ENSO Longitudinal Index (ELI) also uses relative SST, but to estimate the average zonal location of tropical Pacific convection. The Pacific SST zonal gradient index directly measures a key element of ENSO's coupled atmosphere-ocean dynamics. Here, we compared these three modern indices to the traditional Niño-3.4 index, focusing on the relation of their August–October (ASO) values with seasonal Atlantic tropical cyclone activity. We found that the modern ENSO indices outperformed the traditional Niño-3.4 index in nearly all aspects.

The modern indices have higher correlations (across four SST datasets) during the satellite era 1979–2024 with three measures of Atlantic seasonal tropical cyclone activity: accumulated cyclone energy (ACE), number of tropical storms, and number of hurricanes (Fig. 3). The modern indices also show stronger associations during this period with a tropical cyclone genesis potential index (GPI) over the Atlantic (Figure 2). In terms of the environments that appear

in GPI, the modern indices show an advantage over Niño-3.4 in terms of MDR-averaged correlation for vertical wind shear (with the strongest contribution from upper level zonal winds), potential intensity, and absolute vorticity. Of the ENSO indices, relative Niño-3.4 shows the strongest MDR-averaged correlations with GPI and its constituent environments. Consistent with the enhanced response in the Atlantic, the modern indices have stronger correlations with central Pacific convection (Fig. 1).

A challenge in rigorously comparing ENSO indices is their high correlation with each other. One implication of this high degree of similarity is that the traditional Niño-3.4 index, despite its simple formulation, contains nearly the same information as do the modern indices, at least on average. For instance, the high correlation of ELI with Niño-3.4 means that more than 92% of the longitudinal variance of tropical convection represented in ASO ELI is implicitly explained by the traditional Niño-3.4 measure of ENSO strength. To compare the correlations of Atlantic tropical cyclone activity with the modern ENSO indices to that of Niño-3.4, we noted that comparing correlations is equivalent to comparing line fits and applied the Wilcoxon signed-rank test to decide whether the (paired) squared errors differ systematically more than would be expected by chance. Figure S13 illustrates the signed rank sums underlying the p-values in Figure 3. The test results indicate that the advantage of relative Niño-3.4 over Niño-3.4 with Atlantic seasonal tropical cyclone activity (three metrics and four SST datasets) is statistically significant at the 5% level in 10 out of 12 cases and at the 10% level in the remaining two cases (Figs. 3, S10–S12). The corresponding numbers of significant results for the Pacific gradient and ELI are two (5% level) and six (10% level), and five (5% level) and two (10% level), respectively.

For forecast applications, good index performance, i.e., strong relations between simultaneous index values and quantities of interest, is insufficient—the index also must be predictable. Otherwise, the good performance of an index may be undermined by an inability to predict it skillfully. The issue of forecast skill is especially relevant for Atlantic tropical cyclone applications since ENSO forecast skill is relatively low for ASO targets (L'Heureux et al., 2020). We examined the skill with which the North American Multimodel Ensemble (NMME) predicts ASO values of the ENSO indices and the corresponding skill of index-based forecasts of Atlantic tropical cyclone activity. We found that at short leads (June, July, and August starts) all the ENSO indices are forecast with roughly similar skill that fails to match that of persistence. For starts prior to June, forecasts of the modern ENSO indices have skill that matches or surpasses that of the Niño-3.4 index, with forecasts of relative Niño-3.4 and ELI having significantly higher skill than that of Niño-3.4. ENSO index-based forecasts of Atlantic tropical cyclone activity show sta-

tistically significant correlations for forecasts made as early as February, with relative Niño-3.4 having the highest correlation at most lead times and ELI and Niño-3.4 having the lowest.

Although the analysis here has shown advantages of the modern ENSO indices over the period 1979–2024, there is some reason to speculate that the advantage of the modern indices might increase in the future. Despite the similarity of ASO values of the ENSO indices, the difference between Niño-3.4 and the modern ENSO indices is increasing with time, and that trend is statistically significant and robust across SST datasets (Fig. S2). This increasing difference might explain why none of the modern ENSO indices show a particular advantage in terms of their correlation with GPI during the earlier period 1950–1978 (Figs. S14, S15) or with Atlantic tropical cyclone activity measures over the earlier period (Figs. S16–S19). The weaker relation of Niño-3.4 with Atlantic tropical cyclone activity during the pre-satellite era might reflect data quality issues since correlations with GPI are comparable.

The findings here suggest several potential directions for future research. The performance of ENSO indices could be compared in other tropical cyclone measures (e.g., intensity and intensification; Klotzbach, 2012; Tippett & Camargo, 2025) and in other basins where ENSO influences tropical cyclone activity (e.g., western North Pacific). The approaches used here could be applied to other quantities modulated by ENSO (e.g., North American near-surface temperature and precipitation). ENSO indices and their teleconnections could be compared in model data where model biases likely are present but where sampling variability can be reduced by increasing ensemble size.

Data Availability Statement

COBE-SST 2 and Sea Ice (COBE2) and NOAA Extended Reconstructed SST V5 (ERSSTv5) data are provided by the NOAA PSL, Boulder, Colorado, USA, from their website at `https://downloads.psl.noaa.gov/Datasets/COBE2/sst.mon.mean.nc` and `https://downloads.psl.noaa.gov/Datasets/noaa.ersst.v5/sst.mnmean.nc`, respectively. HADISST data are available at `https://www.metoffice.gov.uk/hadobs/hadisst/data/download.html`. The ERA5 reanalysis data set (Hersbach et al., 2020) is available at the Copernicus Climate Change Service, Climate Data Store (2025). The IBTrACS data set (Knapp et al., 2010; Gahtan et al., 2024) is available from the NOAA National Centers for Environmental Information (NCEI) (2025). NMME data are available from the IRI Data Library `https://iridl.ldeo.columbia.edu/SOURCES/.Models/.NMME/`. OLR-Monthly CDR Prod-

uct (Ver03Rev00) data were downloaded from `http://olr.umd.edu/CDR/Monthly/v03r00/OLR-Monthly_v03r00_s197901_latest.nc`.

Acknowledgments

Support from NSF is acknowledged by SJC and CYL (AGS 22-44918 and AGS 22-17618) and EJB (2223262). The scientific results and conclusions, as well as any view or opinions expressed herein, are those of the authors and do not necessarily reflect the views of NWS, NOAA, or the Department of Commerce.

References

Barnston, A. G., Chelliah, M., & Goldenberg, S. B. (1997). Documentation of a highly ENSO-related SST region in the equatorial Pacific. *Atmosphere-Ocean*, *35*, 367-383.

Becker, E. J., Kirtman, B. P., L'Heureux, M., Muñoz, Á. G., & Pegion, K. (2022). A decade of the North American Multimodel Ensemble (NMME): Research, application, and future directions. *Bulletin of the American Meteorological Society*, *103*, E973–E995.

Bister, M., & Emanuel, K. A. (2002). Low frequency variability of tropical cyclone potential intensity. 1. Interannual to interdecadal variability. *J. Geophys. Res.*, *107*, 4801. doi: 10.1029/2001JD000776

Camargo, S. J., Emanuel, K. A., & Sobel, A. H. (2007). Use of a genesis potential index to diagnose ENSO effects on tropical cyclone genesis. *Journal of Climate*, *20*, 4819-4834.

Capotondi, A., Wittenberg, A. T., Newman, M., Di Lorenzo, E., Yu, J.-Y., Braconnot, P., ... Yeh, S.-W. (2014). Understanding ENSO diversity. *Bulletin of the American Meteorological Society*, *96*, 921–938. doi: 10.1175/BAMS-D-13-00117.1

Copernicus Climate Change Service, Climate Data Store. (2025). ERA5 monthly averaged data on pressure levels from 1940 to present [Dataset]. *Copernicus Climate Change Service (C3S) Climate Data Store (CDS)*. doi: 10.24381/cds.6860a573

DelSole, T., & Tippett, M. K. (2014). Comparing forecast skill. *Monthly Weather Review*, *142*, 4658–4678. doi: 10.1175/MWR-D-14-00045.1

Emanuel, K. A., & Nolan, D. S. (2004). Tropical cyclone activity and global climate. In *Proc. of 26th conference on hurricanes and tropical meteorology* (p. 240-241). Miami, FL.

Fueglistaler, S., Radley, C., & Held, I. M. (2015). The distribution of precipitation and the

spread in tropical upper tropospheric temperature trends in CMIP5/AMIP simulations. *Geophysical Research Letters*, *42*, 6000–6007.

Gahtan, J., Knapp, K. R., Schreck, C. J., Diamond, H. J., Kossin, J. P., & Kruk, M. C. (2024). *International Best Track Archive for Climate Stewardship (IBTrACS) Project, Version 4r01*. NOAA. doi: 10.25921/82ty-9e16

Goldenberg, S. B., & Shapiro, L. J. (1996). Physical mechanisms for the association of El Niño and West African rainfall with Atlantic major hurricane activity. *Journal of Climate*, *9*, 1169–1187.

Gray, W. M., Landsea, C. W., Mielke Jr, P. W., & Berry, K. J. (1993). Predicting Atlantic basin seasonal tropical cyclone activity by 1 August. *Weather and Forecasting*, *8*, 73–86.

Hersbach, H., Bell, B., Berrisford, P., Hirahara, S., Horányi, A., Muñoz-Sabater, J., ... others (2020). The ERA5 global reanalysis. *Quarterly Journal of the Royal Meteorological Society*, *146*, 1999–2049. doi: 10.1002/qj.3803

Hirahara, S., Ishii, M., & Fukuda, Y. (2014). Centennial-scale sea surface temperature analysis and its uncertainty. *Journal of Climate*, *27*, 57–75.

Hoell, A., & Funk, C. (2013). The ENSO-related west Pacific sea surface temperature gradient. *Journal of Climate*, *26*, 9545–9562.

Huang, B., Thorne, P. W., Banzon, V. F., Boyer, T., Chepurin, G., Lawrimore, J. H., ... Zhang, H.-M. (2017). Extended reconstructed sea surface temperature, version 5 (ERSSTv5): Upgrades, validations, and intercomparisons. *Journal of Climate*, *30*, 8179–8205. doi: 10.1175/JCLI-D-16-0836.1

Izumo, T., Vialard, J., Lengaigne, M., & Suresh, I. (2020). Relevance of relative sea surface temperature for tropical rainfall interannual variability. *Geophysical Research Letters*, *47*, e2019GL086182.

Kao, H.-Y., & Yu, J.-Y. (2009). Contrasting eastern-Pacific and central-Pacific types of ENSO. *Journal of Climate*, *22*, 615–632.

Kirtman, B., Min, D., Infanti, J. M., Kinter, J. L., III, Paolino, D. A., Zhang, Q., ... Wood, E. F. (2014). The North American Multi-Model Ensemble (NMME): Phase-1 seasonal to interannual prediction, Phase-2 toward developing intra-seasonal prediction. *Bulletin of the American Meteorological Society*, *95*, 585–601. doi: 10.1175/BAMS-D-12-00050.1

Klotzbach, P. J. (2007). Revised prediction of seasonal Atlantic basin tropical cyclone activ-

ity from 1 August. *Weather and Forecasting*, *22*, 937–949.

Klotzbach, P. J. (2012). El Niño-Southern Oscillation, the Madden-Julian Oscillation and Atlantic basin tropical cyclone rapid intensification. *Journal of Geophysical Research: Atmospheres*, *117*, D14104.

Klotzbach, P. J., Bell, G. D., Blake, E. S., & Landsea, C. W. (2017). Seasonal tropical cyclone forecasting. In C. Guard (Ed.), *Global guide to tropical cyclone forecasting* (p. Chapter 7). Geneva, Switzerland: World Meteorological Organization. (Available online at the WMO Tropical Cyclone Programme)

Klotzbach, P. J., Jones, J. J., Wood, K. M., Bell, M. M., Blake, E. S., Bowen, S. G., … Truchelut, R. E. (2024). The 2023 Atlantic hurricane season: An above-normal season despite strong El Niño conditions. *Bulletin of the American Meteorological Society*, *105*(9), E1644–E1661. doi: 10.1175/BAMS-D-23-0305.1

Klotzbach, P. J., Wood, K. M., Bell, M. M., Blake, E. S., Bowen, S. G., Caron, L.-P., … Truchelut, R. E. (2022). A hyperactive end to the Atlantic hurricane season October–November 2020. *Bulletin of the American Meteorological Society*, *103*, E110–E128.

Klotzbach, P. J., Wood, K. M., Schreck III, C. J., Bowen, S. G., Patricola, C. M., & Bell, M. M. (2022). Trends in global tropical cyclone activity: 1990–2021. *Geophysical Research Letters*, *49*, e2021GL095774.

Knapp, K. R., Kruk, M. C., Levinson, D. H., Diamond, H. J., & Neumann, C. J. (2010). The International Best Track Archive for Climate Stewardship (IBTrACS). *Bulletin of the American Meteorological Society*, *91*, 363-376. doi: 10.1175/2009BAMS2755.1

Kousky, V. E., & Higgins, R. W. (2007). An alert classification system for monitoring and assessing the ENSO cycle. *Weather and Forecasting*, *22*, 353-371.

Lee, H.-T., Gruber, A., Ellingson, R. G., & Laszlo, I. (2007). Development of the HIRS outgoing longwave radiation climate dataset. *Journal of Atmospheric and Oceanic Technology*, *24*, 2029–2047.

Lee, S., L'Heureux, M., Wittenberg, A. T., Seager, R., O'Gorman, P. A., & Johnson, N. C. (2022). On the future zonal contrasts of equatorial Pacific climate: Perspectives from observations, simulations, and theories. *npj Climate and Atmospheric Science*, *5*, 82.

L'Heureux, M. L., Levine, A., Newman, M., Ganter, C., Luo, J.-J., Tippett, M. K., & Stockdale, T. (2020). ENSO Prediction. In M. McPhaden, A. Santoso, & W. Cai (Eds.), *El Niño-Southern Oscillation (ENSO) in a Changing Climate.* AGU.

L'Heureux, M. L., Tippett, M. K., & Barnston, A. G. (2015). Characterizing ENSO coupled

variability and its impact on North American seasonal precipitation and temperature. *Journal of Climate*, *28*, 4231-4245. doi: 10.1175/JCLI-D-14-00508.1

L'Heureux, M. L., Tippett, M. K., Wheeler, M. C., Nguyen, H., Narsey, S., Johnson, N., ... others (2024). A relative sea surface temperature index for classifying ENSO events in a changing climate. *Journal of Climate*, *37*, 1197–1211. doi: 10.1175/JCLI-D-23-0406.1

Li, X., Hu, Z.-Z., Ding, R., & Liu, Y. (2023). Which ENSO index best represents its global influences? *Climate Dynamics*, *61*, 4899–4913.

Lin, I.-I., Camargo, S. J., Patricola, C. M., Boucharel, J., Chand, S., Klotzbach, P., ... Jin, F.-F. (2020). ENSO and tropical cyclones. In M. McPhaden, A. Santoso, & W. Cai (Eds.), *El Niño-Southern Oscillation (ENSO) in a Changing Climate.* AGU.

NOAA National Centers for Environmental Information (NCEI). (2025). International Best Track Archive for Climate Stewardship (IBTrACS), Version 4r01. doi: 10.25921/82ty-9e16

Rayner, N., Parker, D. E., Horton, E., Folland, C. K., Alexander, L. V., Rowell, D., ... Kaplan, A. (2003). Global analyses of sea surface temperature, sea ice, and night marine air temperature since the late nineteenth century. *Journal of Geophysical Research: Atmospheres*, *108*.

Saunders, M., Klotzbach, P., Lea, A., Schreck, C., & Bell, M. (2020). Quantifying the probability and causes of the surprisingly active 2018 North Atlantic hurricane season. *Earth and Space Science*, *7*, e2019EA000852.

Seager, R., Henderson, N., & Cane, M. (2022). Persistent discrepancies between observed and modeled trends in the tropical Pacific Ocean. *Journal of Climate*, *35*, 4571-4584. doi: 10.1175/JCLI-D-21-0648.1

Sobel, A. H., Held, I. M., & Bretherton, C. S. (2002). The ENSO signal in tropical tropospheric temperature. *Journal of Climate*, *15*, 2702–2706.

Sobel, A. H., Lee, C.-Y., Bowen, S. G., Camargo, S. J., Cane, M. A., Clement, A., ... Tippett, M. K. (2023). Near-term tropical cyclone risk and coupled Earth system model biases. *Proceedings of the National Academy of Sciences*, *120*, e2209631120.

Swanson, K. L. (2008). Nonlocality of Atlantic tropical cyclone intensity. *Geochem. Geophys. Geosyst.*, *9*, Q04V01.

Tang, B. H., & Neelin, J. (2004). ENSO influence on Atlantic hurricanes via tropospheric warming. *Geophysical Research Letters*, *31*, L24204. doi: 10.1029/2004GL021072

Tippett, M. K., & Camargo, S. J. (2025). Trends and ENSO-related variability in Atlantic tropical cyclone intensity and intensification. *Journal of Climate*. doi: 10.1175/JCLI-D-25-0106.1

Van Oldenborgh, G. J., Hendon, H., Stockdale, T., L'Heureux, M., De Perez, E. C., Singh, R., & Van Aalst, M. (2021). Defining El Niño indices in a warming climate. *Environmental Research Letters*, *16*, 044003.

Vecchi, G. A., Zhao, M., Wang, H., Villarini, G., Rosati, A., Kumar, A., … Gudgel, R. (2010). Statistical–Dynamical Predictions of Seasonal North Atlantic Hurricane Activity. *Monthly Weather Review*, *139*, 1070–1082. doi: 10.1175/2010MWR3499.1

Villarini, G., Vecchi, G. A., & Smith, J. A. (2010). Modeling of the dependence of tropical storm counts in the North Atlantic basin on climate indices. *Monthly Weather Review*, *138*, 2681-2705. doi: 10.1175/2010MWR3315.1

Watanabe, M., Dufresne, J.-L., Kosaka, Y., Mauritsen, T., & Tatebe, H. (2021). Enhanced warming constrained by past trends in equatorial Pacific sea surface temperature gradient. *Nature Climate Change*, *11*, 33–37.

Williams, I. N., & Patricola, C. M. (2018). Diversity of ENSO events unified by convective threshold sea surface temperature: A nonlinear ENSO index. *Geophysical Research Letters*, *45*, 9236–9244.

Supporting information for "Relation of Atlantic tropical cyclone activity with observed and predicted ENSO indices"

Michael K. Tippett[1], Emily J. Becker[2], Suzana J. Camargo[3], Jorge L. García-Franco[4], Chia-Ying Lee[5], Michelle L. L'Heureux[6]

[1]Department of Applied Physics and Applied Mathematics, Columbia University, New York, NY, USA

[2]University of Miami Rosenstiel School for Marine, Earth, and Atmospheric Science, Miami, FL, USA

[3]Columbia Climate School, Columbia University, New York, NY, USA

[4]Escuela Nacional de Ciencias de la Tierra, UNAM, Mexico

[5]Lamont-Doherty Earth Observatory, Columbia University, Palisades, NY, USA

[6]NOAA/NWS/NCEP/Climate Prediction Center, College Park, MD, USA

Contents of this file

1. Figures S1 to S19

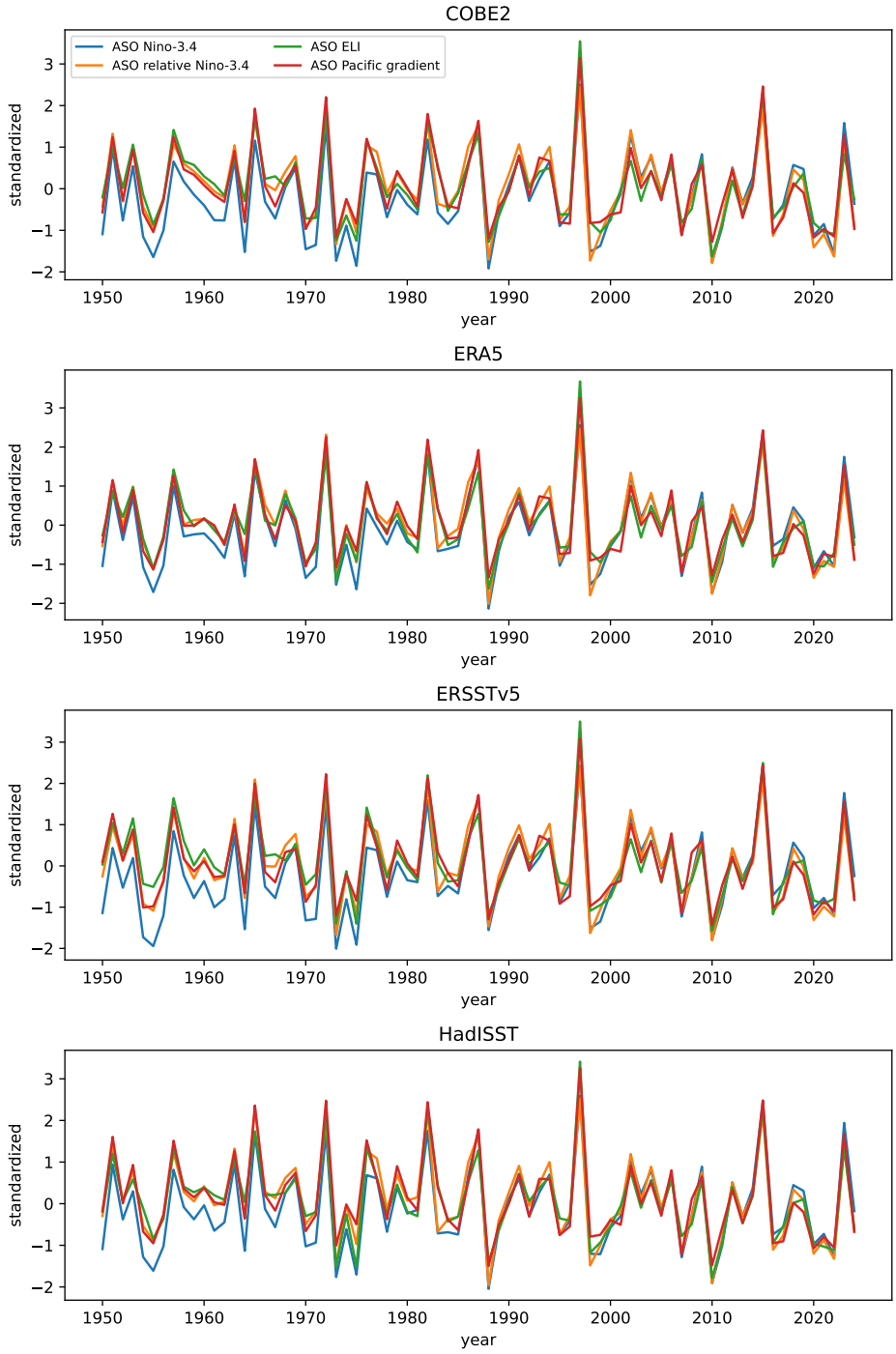

Figure S1. ENSO indices 1950–2024 (standardized by 1991–2020 values) in four SST datasets.

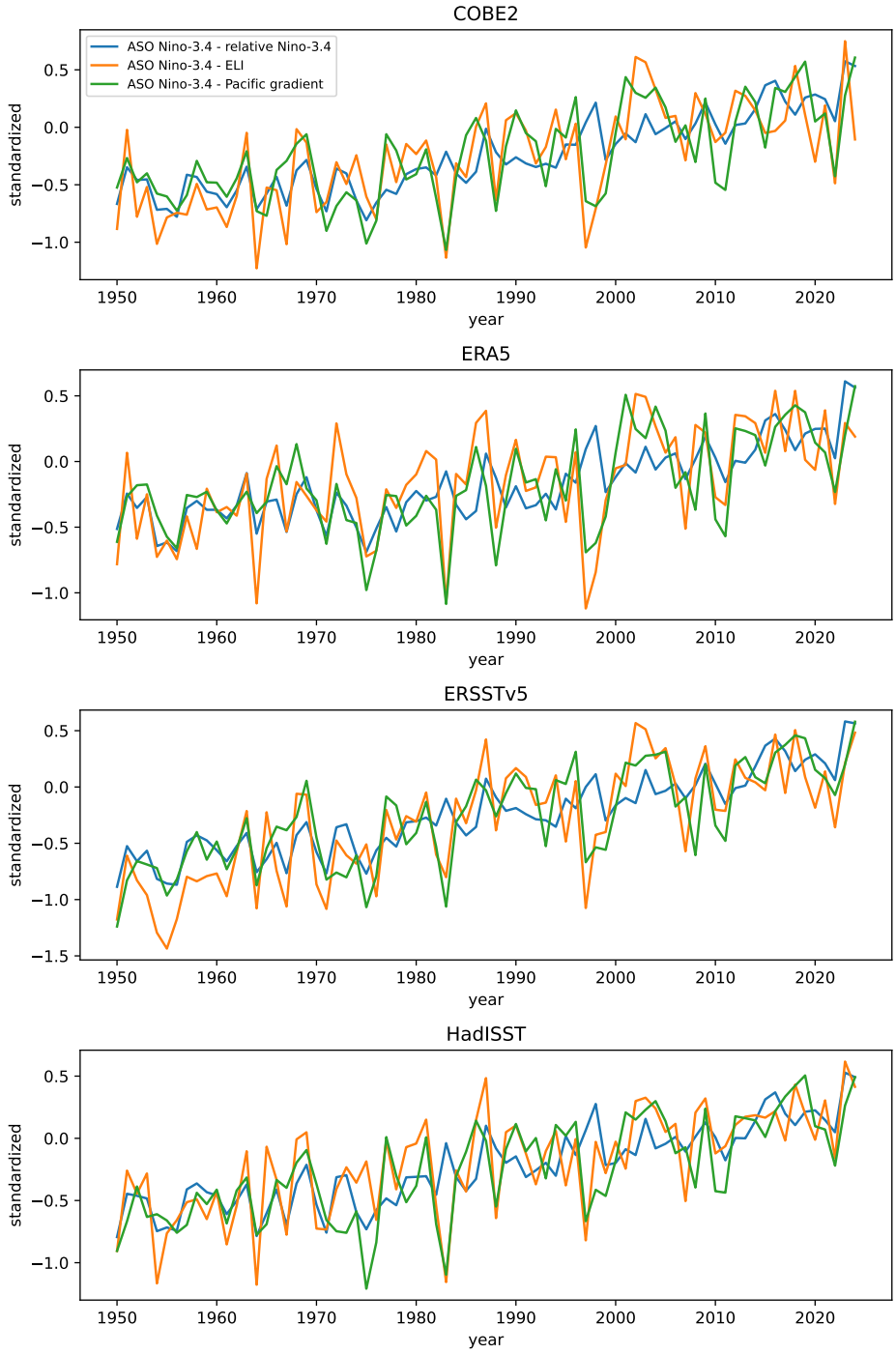

Figure S2. Differences of Niño-3.4 with the modern ENSO indices 1950–2024 (standardized by 1991–2020 values) in four SST datasets.

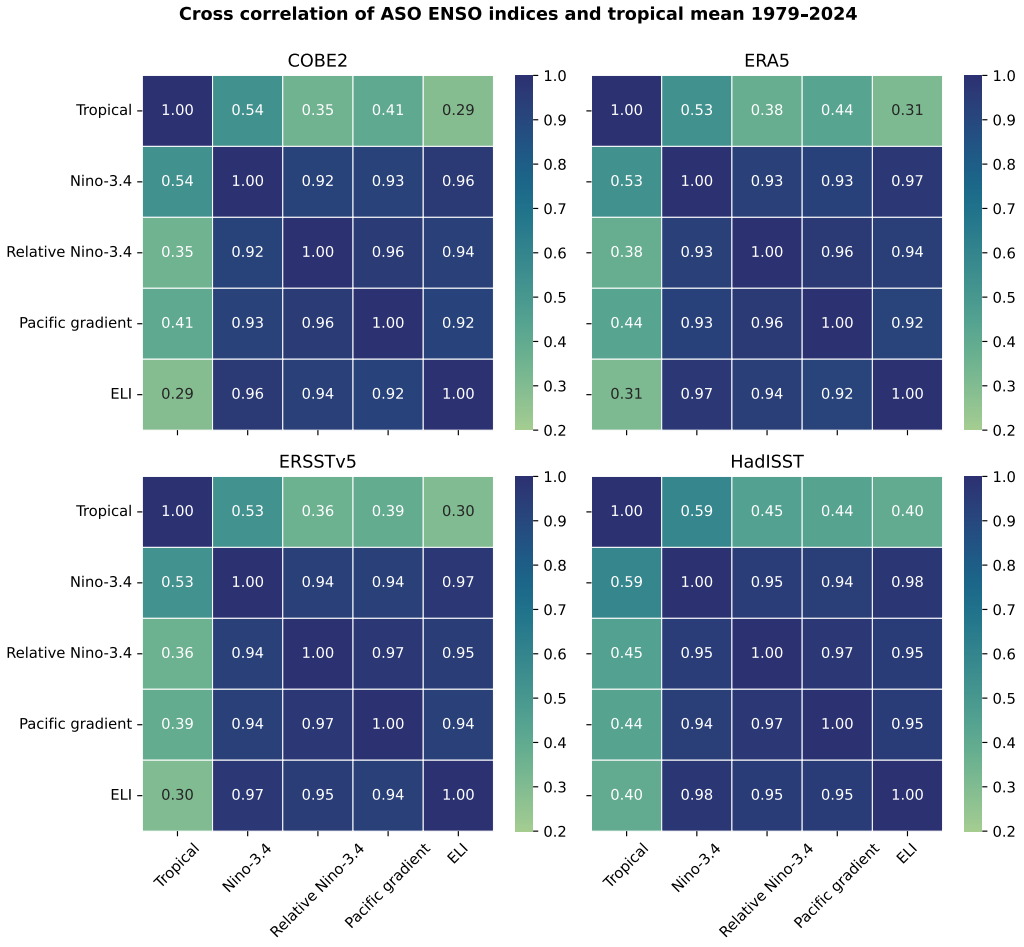

Figure S3. Cross correlation of ASO ENSO indices and tropical mean SST 1979–2024 in four SST datasets.

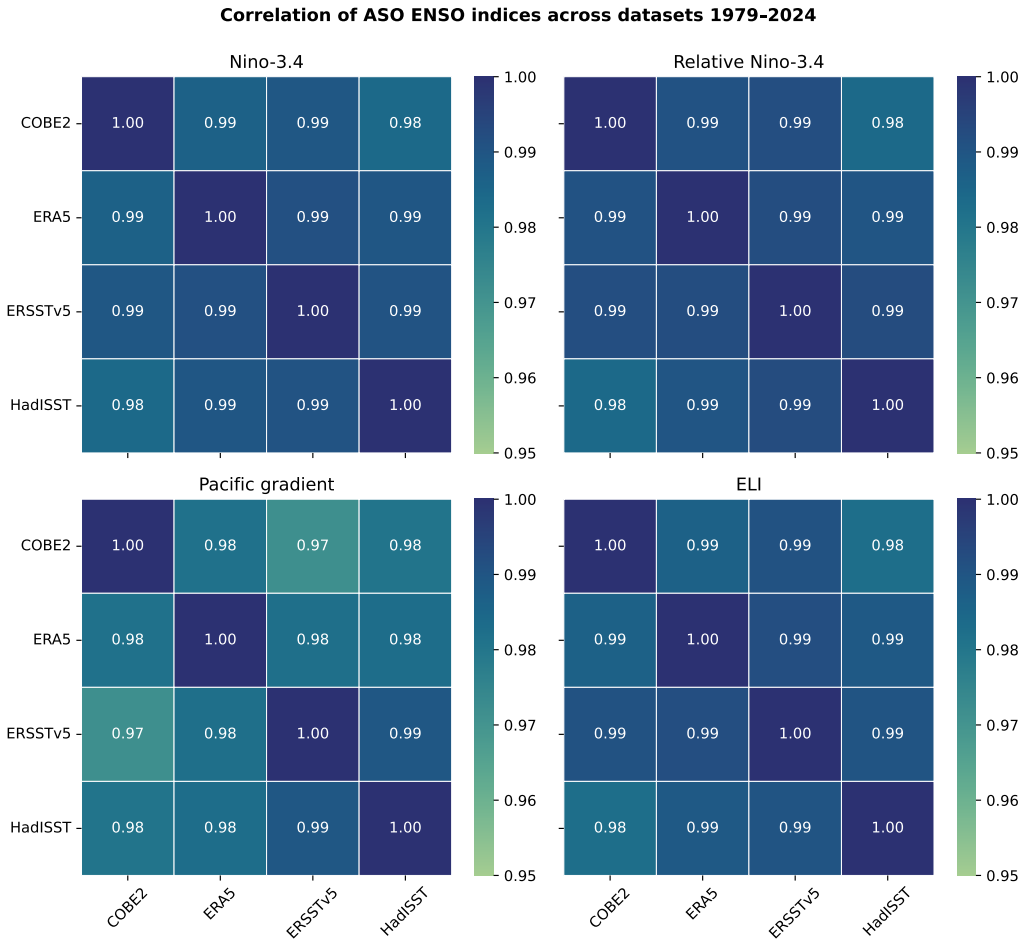

Figure S4. Correlation of ASO ENSO indices across four SST datasets 1979–2024.

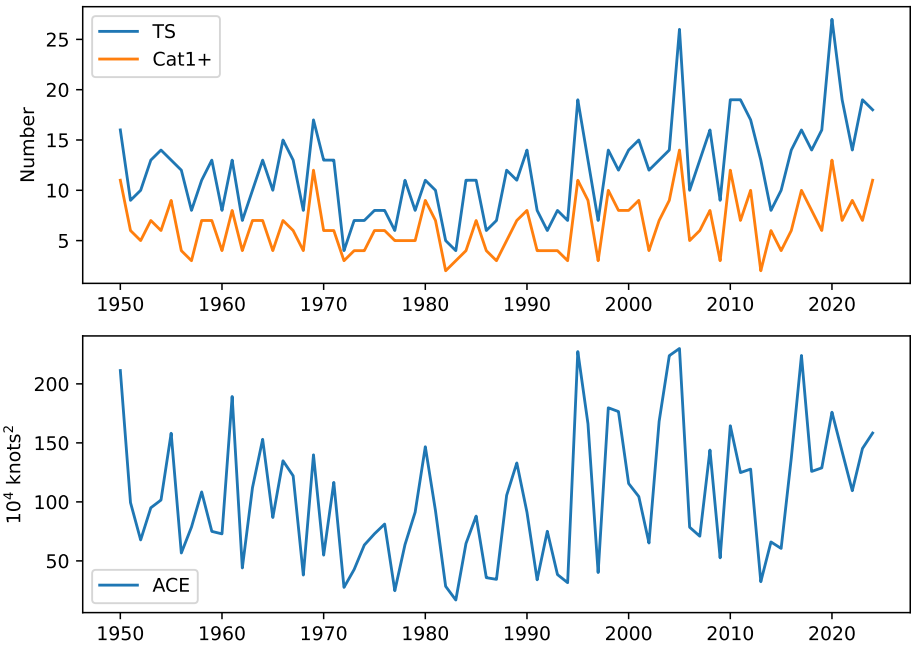

Figure S5. Atlantic tropical cyclone activity indices 1950–2024.

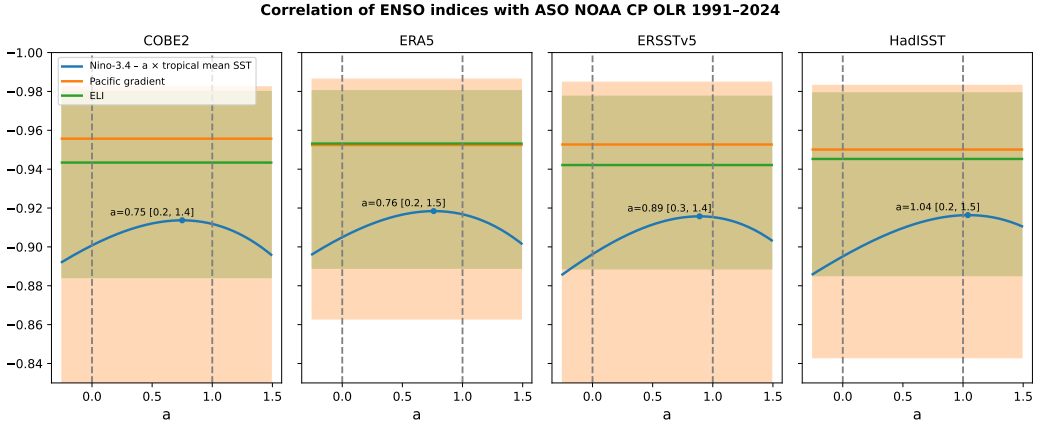

Figure S6. Correlation of ASO CP-OLR with Niño-3.4 - a × tropical mean (blue), ELI (orange), and Pacific gradient (green) during the period **1991–2024** in four SST datasets. Text shows the value of a that maximizes the correlation (marked by a dot) along with 95% confidence intervals. Orange and green shading shows 95% confidence intervals for the Pacific gradient and ELI correlations, respectively.

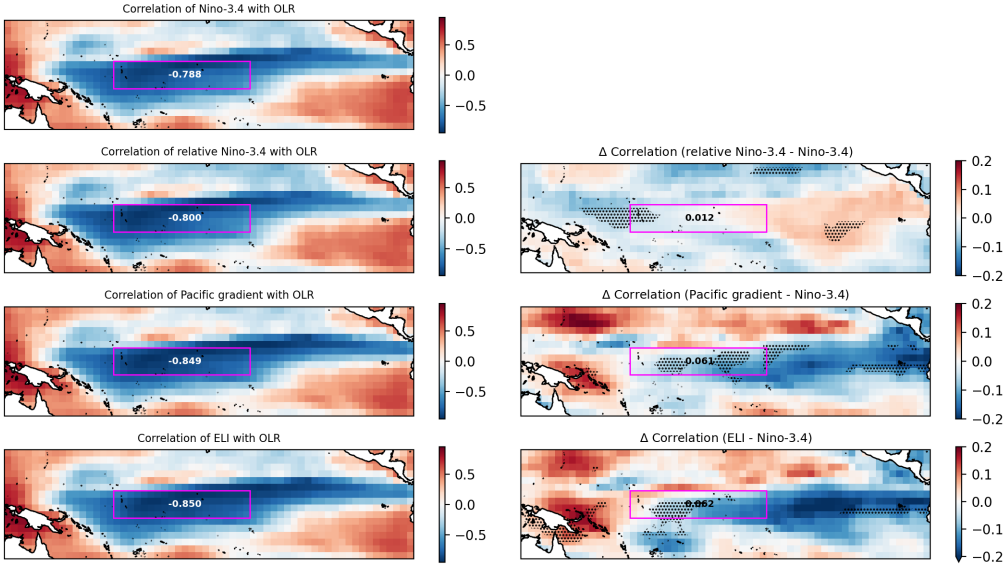

Figure S7. Correlation of ENSO indices with ASO OLR 1979–2024 (left) and their differences from the Niño-3.4 correlation (right). The CP region is outlined in magenta, and the annotated value is the CP average correlation. Stippling shows statistically significant (5% level) differences.

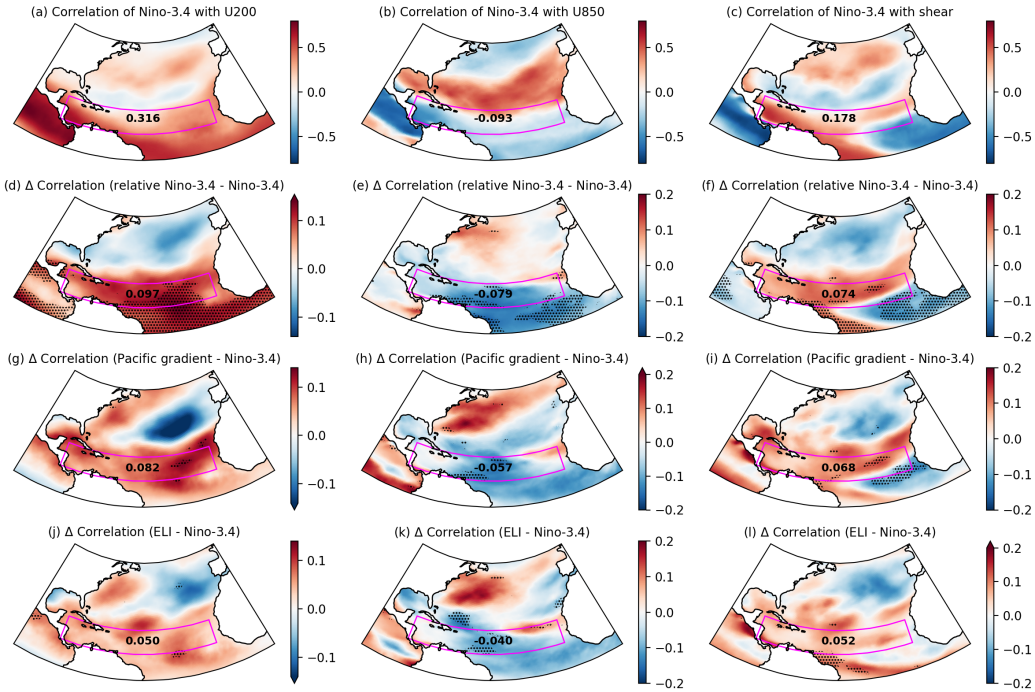

Figure S8. Each column corresponds to one Atlantic environmental variable: **200 hPa zonal wind** (left), **850 hPa zonal wind** (middle), and **vertical wind shear** (right). The top row (a–c) shows the correlation with Niño-3.4 for ASO 1979–2024. Moving down each column, rows 2–4 show the difference in correlation compared to that of Niño-3.4 when using (d–f) relative Niño-3.4, (g–i) Pacific gradient, and (j–l) ELI. The MDR is outlined in magenta; annotated numbers are MDR averages (correlation in row 1, change in correlation in rows 2–4). Stippling marks statistically significant (5%) differences.

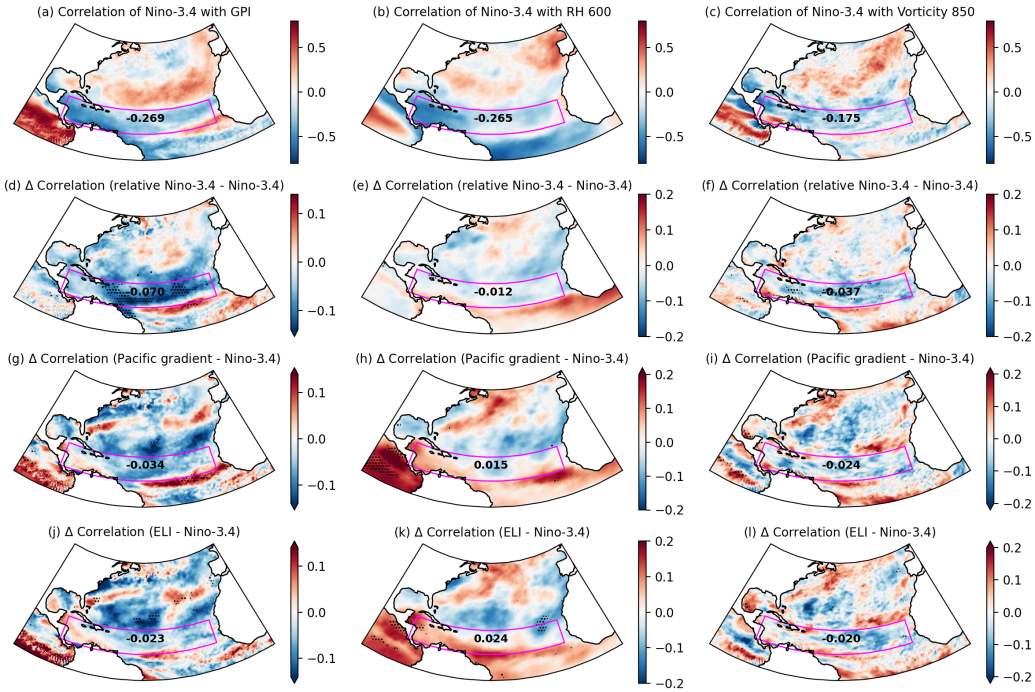

Figure S9. Each column corresponds to one Atlantic environmental variable: **GPI** (left), **600 hPa relative humidity** (middle), and **850 hPa vorticity** (right). The top row (a–c) shows the correlation with Niño-3.4 for ASO 1979–2024. Moving down each column, rows 2–4 show the difference in correlation compared to that of Niño-3.4 when using (d–f) relative Niño-3.4, (g–i) Pacific gradient, and (j–l) ELI. The MDR is outlined in magenta; annotated numbers are MDR averages (correlation in row 1, change in correlation in rows 2–4). Stippling marks statistically significant (5%) differences.

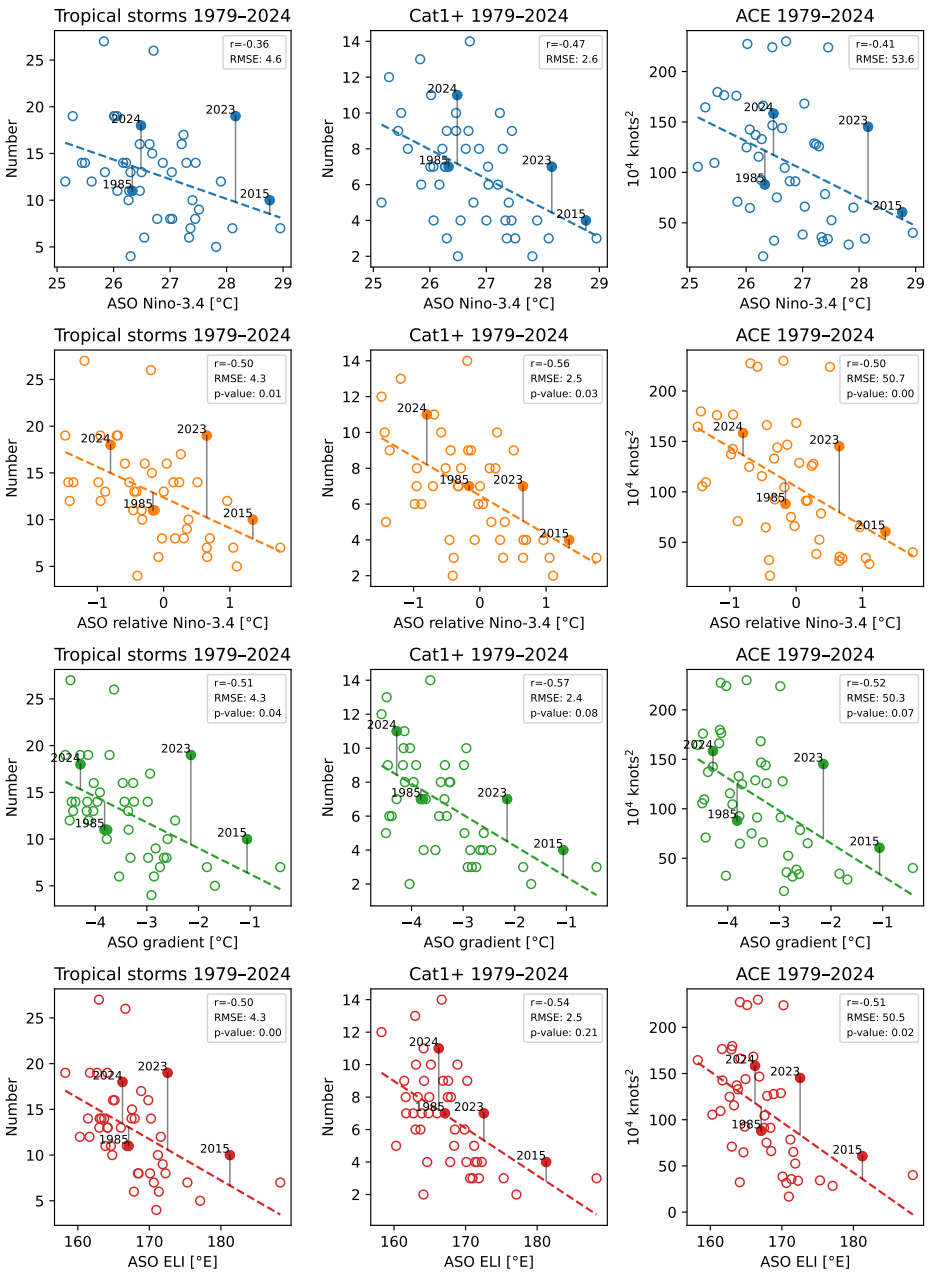

Figure S10. ASO ENSO indices (**COBE2**) with seasonal number of named storms (left column), Cat1+ hurricanes (middle column), and ACE (right column) for the period 1979–2024, along with best-fit lines (dashed). P-values are shown for the null hypothesis that the relation with Niño-3.4 is the same (small values favor rejecting).

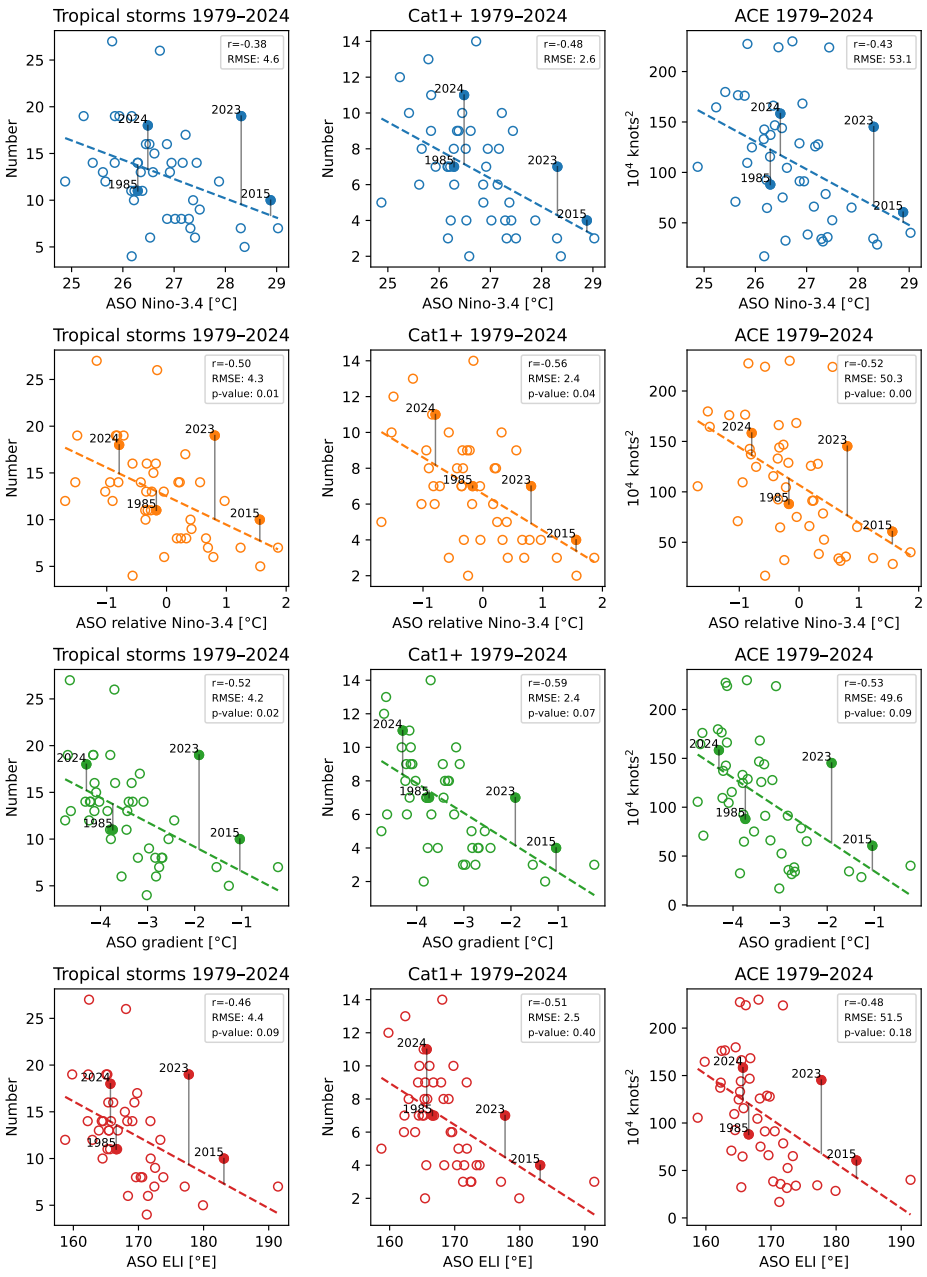

Figure S11. ASO ENSO indices (**ERA5**) with seasonal number of named storms (left column), Cat1+ hurricanes (middle column), and ACE (right column) for the period 1979–2024, along with best-fit lines (dashed). P-values are shown for the null hypothesis that the relation with Niño-3.4 is the same (small values favor rejecting).

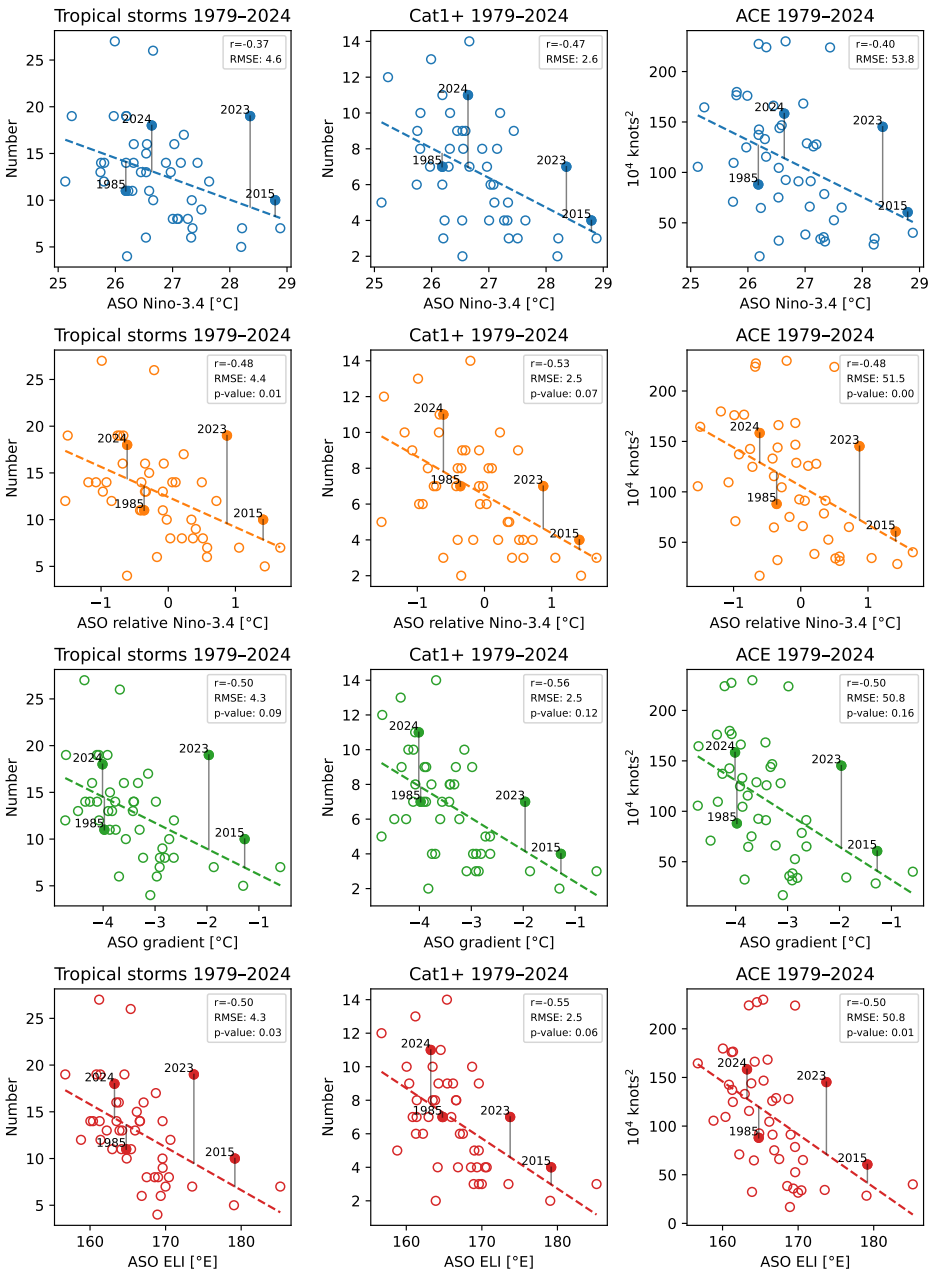

Figure S12. ASO ENSO indices (**HadISST**) with seasonal number of named storms (left column), Cat1+ hurricanes (middle column), and ACE (right column) for the period 1979–2024, along with best-fit lines (dashed). P-values are shown for the null hypothesis that the relation with Niño-3.4 is the same (small values favor rejecting).

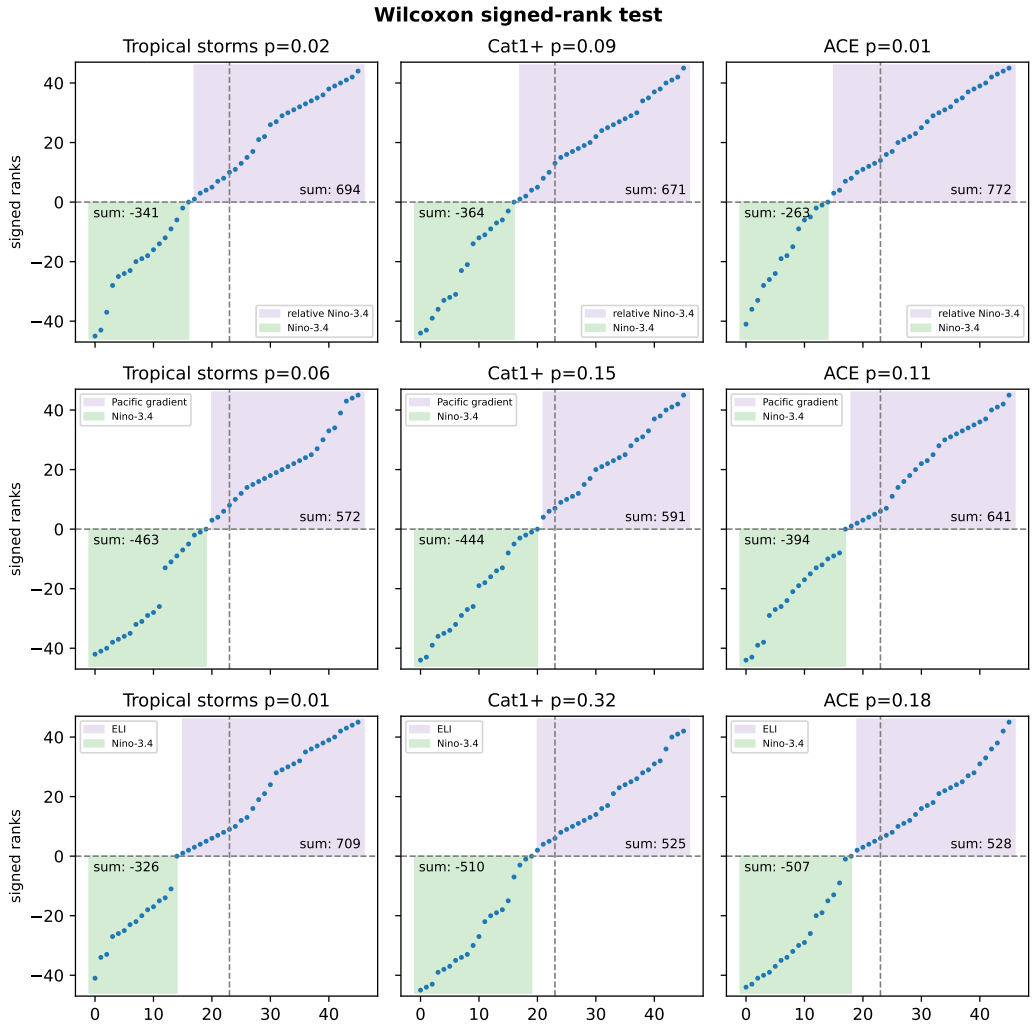

Figure S13. Signed ranks (dots) and their sums (text) of the differences of the squared errors for Niño-3.4 and the modern indices (**ERSSTv5**) for number of Atlantic storms, Cat1+ storms, and ACE. Positive values indicate smaller squared error for the modern index (purple shading), while negative values indicate smaller squared error for Niño-3.4 (green shading). P-values are shown for the null hypothesis that the relation with Niño-3.4 and the modern index is the same (small values favor rejecting).

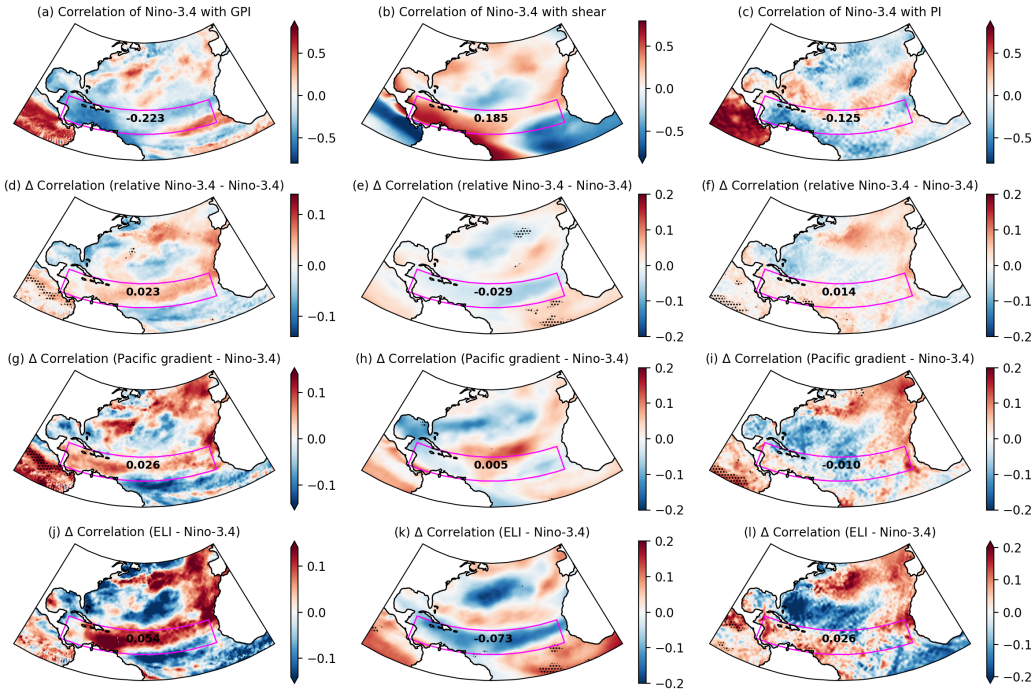

Figure S14. Each column corresponds to one Atlantic environmental variable: **GPI** (left), **vertical wind shear** (middle), and **potential intensity** (PI) (right). The top row (a–c) shows the correlation with Niño-3.4 for ASO **1950–1978**. Moving down each column, rows 2–4 show the difference in correlation compared to that of Niño-3.4 when using (d–f) relative Niño-3.4, (g–i) Pacific gradient, and (j–l) ELI. The MDR is outlined in magenta; annotated numbers are MDR averages (correlation in row 1, change in correlation in rows 2–4). Stippling marks statistically significant (5%) differences.

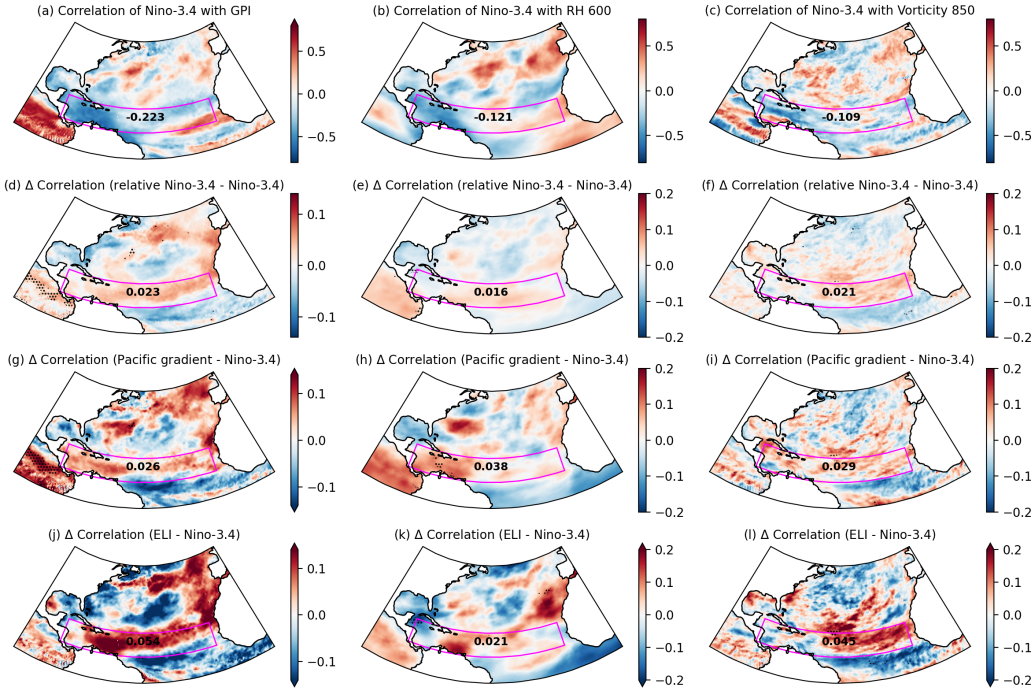

Figure S15. Each column corresponds to one Atlantic environmental variable: **GPI** (left), **600 hPa relative humidity** (middle), and **850 hPa vorticity** (right). The top row (a–c) shows the correlation with Niño-3.4 for ASO **1950–1978**. Moving down each column, rows 2–4 show the difference in correlation compared to that of Niño-3.4 when using (d–f) relative Niño-3.4, (g–i) Pacific gradient, and (j–l) ELI. The MDR is outlined in magenta; annotated numbers are MDR averages (correlation in row 1, change in correlation in rows 2–4). Stippling marks statistically significant (5%) differences.

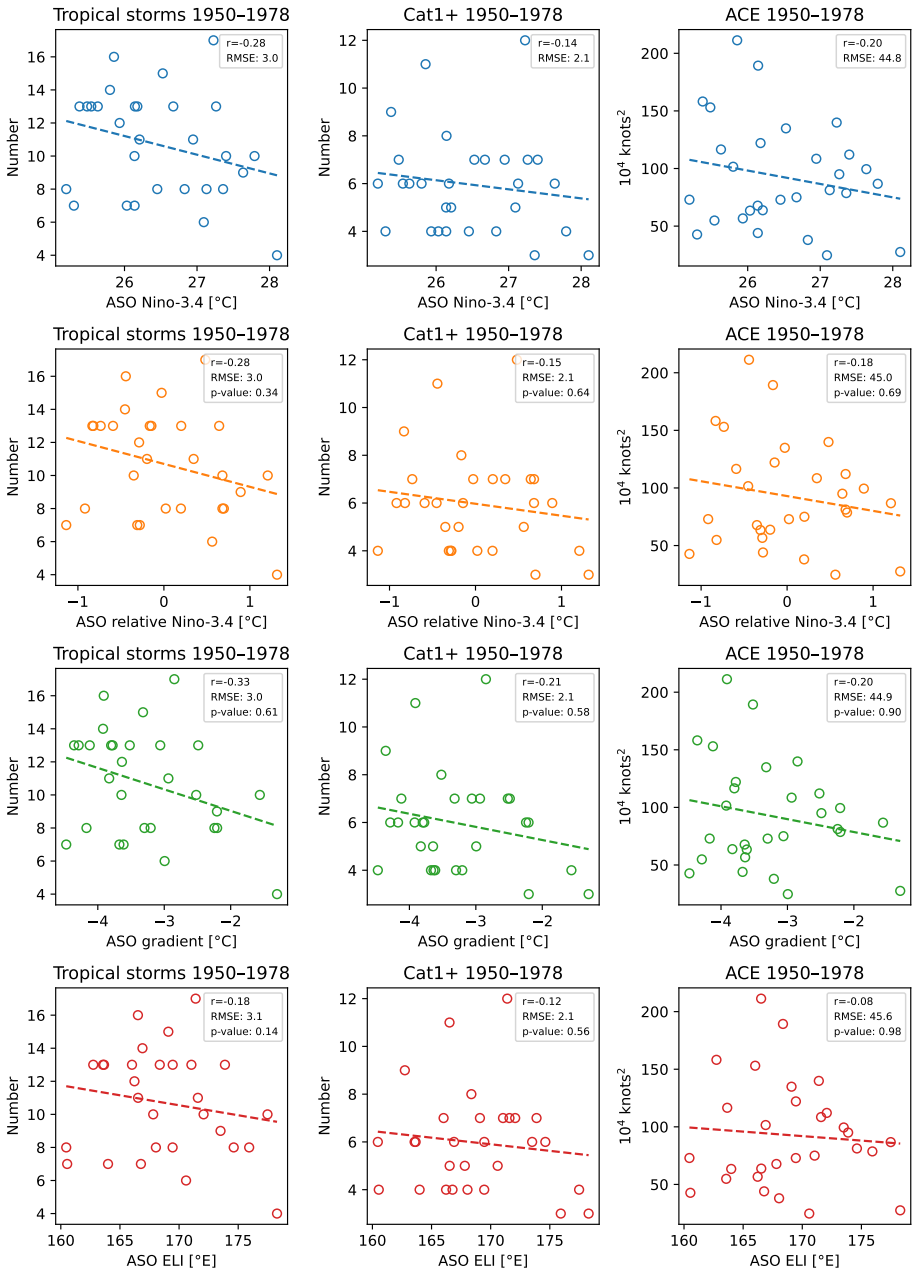

Figure S16. ASO ENSO indices (**COBE2**) with seasonal number of named storms (left column), Cat1+ hurricanes (middle column), and ACE (right column) for the period **1950–1978**, along with best-fit lines (dashed). P-values are shown for the null hypothesis that the relation with Niño-3.4 is the same (small values favor rejecting).

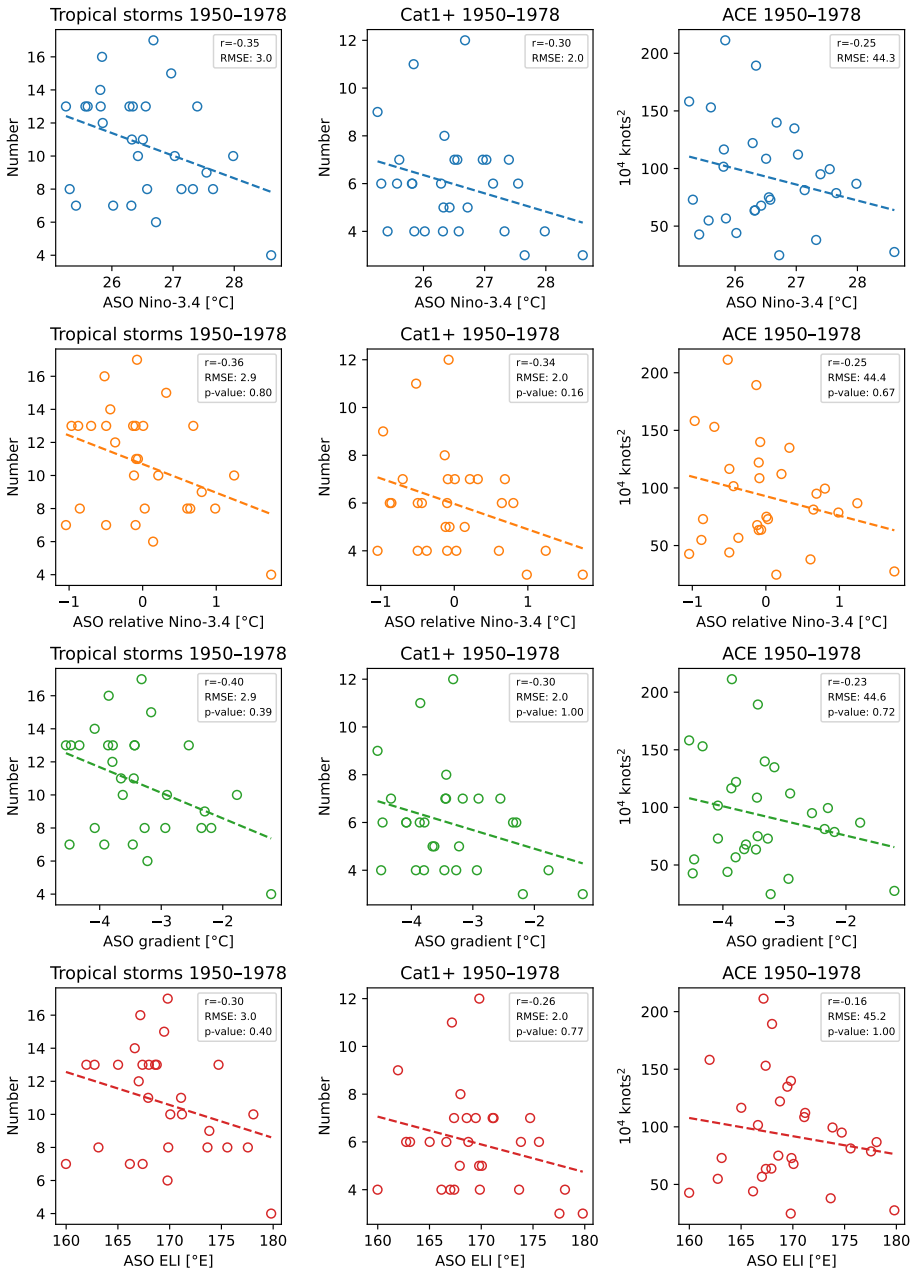

Figure S17. ASO ENSO indices (**ERA5**) with seasonal number of named storms (left column), Cat1+ hurricanes (middle column), and ACE (right column) for the period **1950–1978**, along with best-fit lines (dashed). P-values are shown for the null hypothesis that the relation with Niño-3.4 is the same (small values favor rejecting).

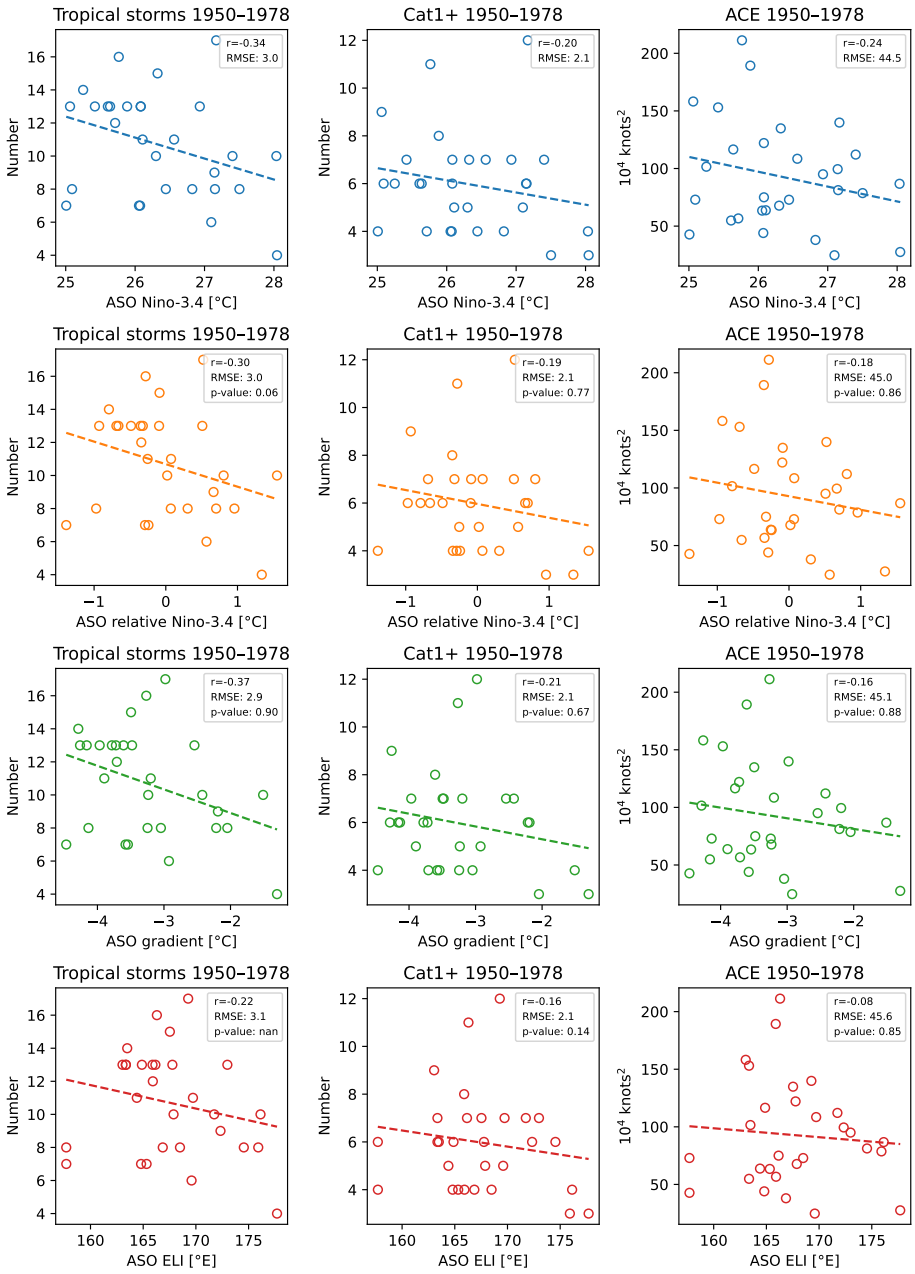

Figure S18. ASO ENSO indices (**ERSSTv5**) with seasonal number of named storms (left column), Cat1+ hurricanes (middle column), and ACE (right column) for the period **1950–1978**, along with best-fit lines (dashed). P-values are shown for the null hypothesis that the relation with Niño-3.4 is the same (small values favor rejecting).

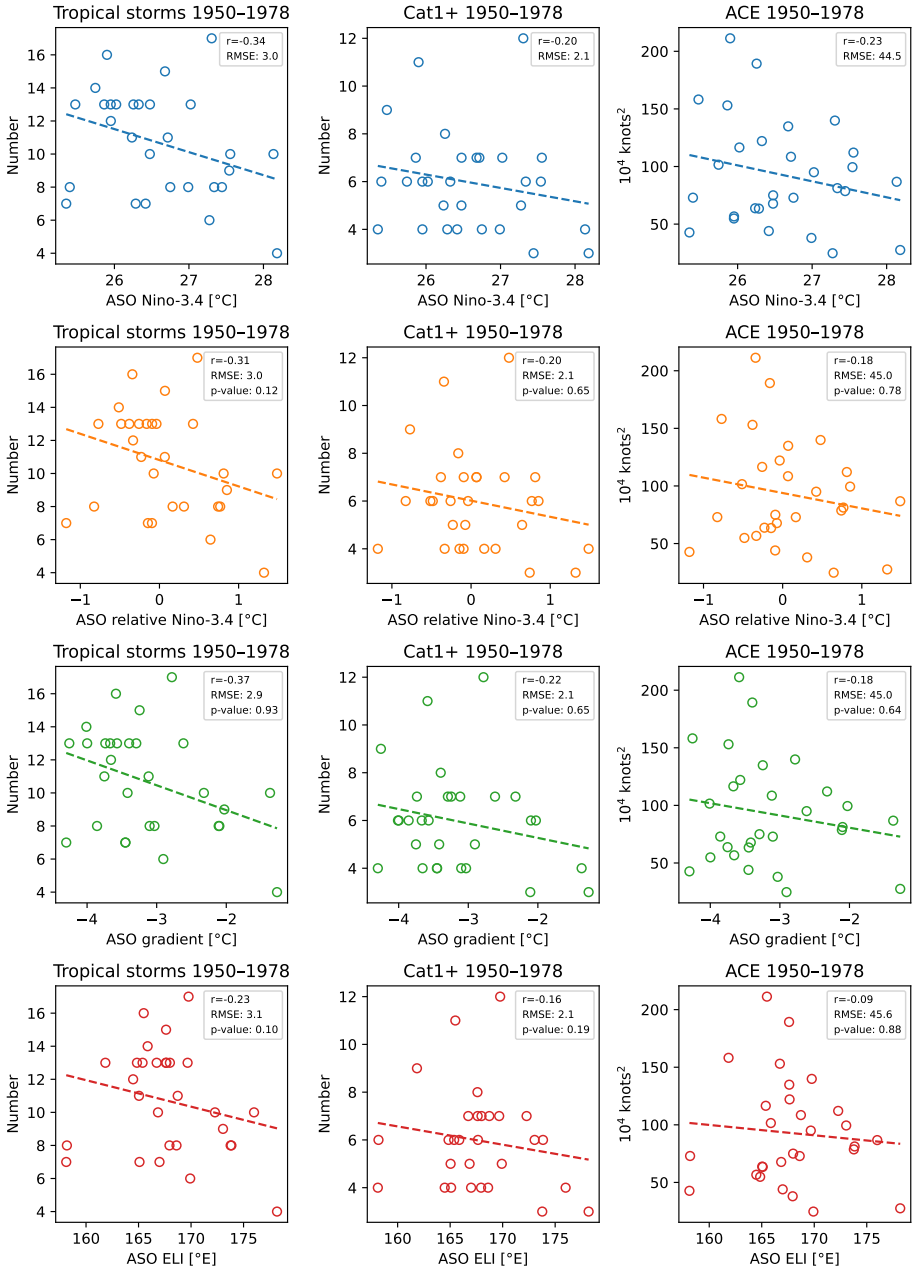

Figure S19. ASO ENSO indices (**HadISST**) with seasonal number of named storms (left column), Cat1+ hurricanes (middle column), and ACE (right column) for the period **1950–1978**, along with best-fit lines (dashed). P-values are shown for the null hypothesis that the relation with Niño-3.4 is the same (small values favor rejecting).